

Discovery of 1,5-Diphenylpyrazole-3-Carboxamide Derivatives as Potent, Reversible, and Selective Monoacylglycerol Lipase (MAGL) Inhibitors

Mojgan Aghazadeh Tabrizi,[§] Pier Giovanni Baraldi,[§] Stefania Baraldi,[§] Emanuela Ruggiero,[§] Lucia De Stefano,^{⊥,ϕ} Flavio Rizzolio,^{‡,ϕ} Lorenzo Di Cesare Mannelli,[⊥] Carla Ghelardini,[⊥] Andrea Chicca,[#] Margherita Lapillo,^{‡,#} Jürg Gertsch,[#] Clementina Manera,[†] Marco Macchia,[†] Adriano Martinelli,[†] Carlotta Granchi,[†] Filippo Minutolo,[†] and Tiziano Tuccinardi^{†,ψ,}*

[§] Department of Chemical and Pharmaceutical Sciences, University of Ferrara, 44121 Ferrara, Italy

[⊥] Graduate School in Chemistry, University of Trieste, 34127 Trieste, Italy

[†] Department of Pharmacy, University of Pisa, 56126 Pisa, Italy

^ϕ Division of Experimental and Clinical Pharmacology, Department of Molecular Biology and Translational Research, National Cancer Institute and Center for Molecular Biomedicine, 33081 Aviano (PN), Italy

[‡] Department of Molecular Science and Nanosystems, Ca' Foscari Università di Venezia, 30172 Venezia-Mestre, Italy

[⊥] Department of Neuroscience, Psychology, Drug Research and Child Health, Section of Pharmacology and Toxicology, University of Firenze, 50139 Firenze, Italy

[#] Institute of Biochemistry and Molecular Medicine, NCCR TransCure, University of Bern, CH-3012 Bern, Switzerland

^ψ Sbarro Institute for Cancer Research and Molecular Medicine, Center for Biotechnology, College of Science and Technology, Temple University, 19122 Philadelphia, PA, USA

ABSTRACT

Monoacylglycerol lipase (MAGL) is a serine hydrolase that plays an important role in the degradation of the endocannabinoid neurotransmitter 2-arachidonoylglycerol, which is implicated in many physiological processes. Beyond the possible utilization of MAGL inhibitors as anti-inflammatory, anti-nociceptive and anti-cancer agents, their application has encountered obstacles due to the unwanted effects caused by the irreversible inhibition of this enzyme. The possible application of reversible MAGL inhibitors has only recently been explored, mainly due to the deficiency of known compounds possessing efficient reversible inhibitory activities. In this work, we report a new series of reversible MAGL inhibitors. Among them, compound **26** showed to be a potent MAGL inhibitor ($IC_{50} = 0.51 \mu\text{M}$, $K_i = 412 \text{ nM}$) with a good selectivity versus fatty acid amide hydrolase (FAAH), α/β -hydrolase domain-containing 6 (ABHD6) and 12 (ABHD12). Interestingly, this compound also possesses antiproliferative activities against two different cancer cell lines and relieves the neuropathic hypersensitivity induced *in vivo* by oxaliplatin.

INTRODUCTION

The endocannabinoid system is characterized by a set of neuromodulatory lipids and their receptors, which are involved in a multiplicity of physiological and pathological conditions. Two different types of G protein-coupled receptors (GPCRs) have been discovered and named as central cannabinoid (CB_1) and peripheral cannabinoid (CB_2) receptors.¹ Endocannabinoid signaling regulates various phases of mammalian physiological processes, including pain perception, feeding, emotional state, learning and memory.²⁻⁴ Endocannabinoids are hypothesized to act as retrograde messengers, where stimulation of the postsynaptic neuron activates the biosynthesis of endocannabinoids, which are released and transported to activate CB_1 receptors expressed mainly in the CNS on the presynaptic terminal.⁵ Endocannabinoids are biosynthesized on demand from phospholipid precursors at the

plasma membrane levels and then released in the extracellular milieu.⁶ After activating the receptors, endocannabinoids are transported into the cytoplasm via facilitated diffusion and degraded by specific enzymes. Several evidence *in vitro* and *in vivo* support the existence of a putative endocannabinoid membrane transporter which mediates the bidirectional movement of endocannabinoids through the plasma membrane^{7, 8} in cooperation with other proteins such as hydrolytic enzymes and intracellular carrier proteins.^{9, 10} The complex enzymatic cascades that regulate endocannabinoid production and inactivation include different hydrolytic enzymes, such as the fatty acid amide hydrolase (FAAH), *N*-acylethanolamine hydrolyzing acid amidase (NAAA) and monoacylglycerol lipase (MAGL).^{3, 11} The selective diacylglycerol lipases (DAGL) α and β are thought to catalyze the formation of 2-arachidonoylglycerol (2-AG), and MAGL degrades this compound into arachidonate and glycerol. Anandamide (AEA) is a partial CB₁ agonist and a weak partial CB₂ agonist, whereas 2-AG acts as a full CB₂ agonist.¹² The 2-AG levels in the brain are about three orders of magnitude higher than AEA levels, although the relevance of this difference on their signaling actions is still uncertain, mainly taking into consideration that their basal extracellular levels, as measured by *in vivo* microdialysis, are within 2- to 5-fold.^{13, 14} In addition to extracellular CB receptors, endocannabinoids interact with other receptors like the vanilloid receptor 1 (VR1), the transient potential vanilloid type 1 channels (TRPV1) and other specific GPCRs such as opioid or GPR55 and GPR35 receptors.¹⁵ The discovery that the endocannabinoids work together with different receptor sites has contributed to the identification of this signaling system as a flexible tool to control diverse functions in the cells and tissues of the organism. Numerous studies suggest the potential use of selective inhibitors implicated in enzymatic degradation of endocannabinoids that could provide selective therapeutic chances.¹⁶ To reduce the problems connected with CB₁ agonists, an amplification of the actions of AEA and 2-AG by inhibiting their enzymatic degradation has emerged as a potential strategy to develop the endocannabinoid system for medicinal purposes. Pharmacological inhibition of FAAH and MAGL was found to decrease pain, inflammation, anxiety, and depression in rodent models without the undesired side effects in motility and behavior observed with direct CB₁ agonists.³ First generation

MAGL inhibitors include URB602 (compound **1**), N-Arachidonoyl maleimide (NAM, compound **2**), and OMDM169 (compound **3**).¹⁷ Carbamate compound **1** (Figure 1) was reported as a MAGL inhibitor with relatively low potency ($IC_{50} = 28 \mu M$)¹⁸ and it was shown to be equally potent against FAAH *in vitro*.^{19, 20} Furthermore, its administration was shown to attenuate nociception in rodent models of acute, inflammatory, and neuropathic pain.^{21, 22} Compound **2** (Figure 1) is an irreversible MAGL inhibitor ($IC_{50} = 140 \text{ nM}$) that was found to decrease 2-AG hydrolase activity of rat cerebellar membranes.²³ NAM is not selective due to its chemically reactive maleimide functional group that will likely react with many cysteine-containing proteins *in vivo*, thus limiting its use in physiologic studies. Another carbamate-based derivative **3** (OMDM169, Figure 1) is a MAGL competitive inhibitor ($IC_{50} = 0.89 \mu M$)²⁴ that increased the 2-AG levels at the site of formalin-induced paw inflammation but it also inhibited pancreatic lipase and DAGL- α , because of its structural similarity with tetrahydrolipstatin. Selective pharmacological tools able to interrupt the *in vivo* MAGL activity have only become accessible within the last few years. By now, they have been used to demonstrate the role of this enzyme in 2-AG signaling termination and the potential translational use of targeting MAGL in the treatment of nervous system disorders such as pain, anxiety, drug addiction, nausea, and neuroinflammation.²⁵⁻²⁷ Furthermore, MAGL is upregulated in aggressive cancer cells and primary tumors and its inhibition in aggressive breast, ovarian and melanoma cancer cells impairs cell migration, invasiveness and tumorigenicity.²⁸ Confirmation of MAGL as the primary brain 2-AG hydrolase was achieved by the generation of a selective and *in vivo* active MAGL inhibitor, JZL184 (**4**, Figure 1). This piperidine carbamate is a potent and selective MAGL inhibitor ($IC_{50} = 8 \text{ nM}$) that when administered to mice, elevated brain 2-AG levels leading to several cannabinoid-related behavioral effects.²⁹ Almost all the reported compounds are characterized by an irreversible MAGL inhibition mechanism and as reported by Scholsburg et al., the irreversible inhibition of MAGL produces cross-tolerance to CB₁ agonists in mice after repeated administrations.³⁰ Furthermore, chronic MAGL blockade causes physical dependence, impairs endocannabinoid-dependent synaptic plasticity and desensitizes brain CB₁ receptors.³⁰ Considering these drawbacks associated with an

irreversible MAGL inhibition, the development of reversible inhibitors could represent a promising alternative strategy; however, their use has been investigated only partially so far, mainly because of the lack of compounds with good MAGL reversible inhibition properties. In 2012 Cisneros et al. reported a series of oxirane derivatives characterized by a dual MAGL/FAAH reversible inhibition activity;³¹ whereas in 2014 Hernandez-Torres et al. reported the reversible MAGL inhibitor benzo[*d*][1,3]dioxol-5-ylmethyl 6-([1,1'-biphenyl]-4-yl)-hexanoate **5** (compound c21, Figure 1). Interestingly, this compound was also tested *in vivo* and its therapeutic effects were not accompanied by catalepsy or other motor impairments that have been observed instead after the administration of irreversible MAGL inhibitors.³² In 2015 Patel et al. developed a series of Loratadine analogues that showed potent and reversible inhibition of MAGL, accompanied also by selectivity towards human FAAH. Furthermore, one of these derivatives proved to possess antagonistic activity towards the Histamine H1 receptor and showed selectivity against cannabinoid receptors, α/β -hydrolase domain-containing 6 (ABHD6) and α/β -hydrolase domain-containing 12 (ABHD12).³³ Finally, very recently Granchi et al. reported a benzoylpiperidine derivative characterized by a good MAGL inhibitory activity ($IC_{50} = 0.84 \mu M$) and a reversible mechanism of inhibition.³⁴

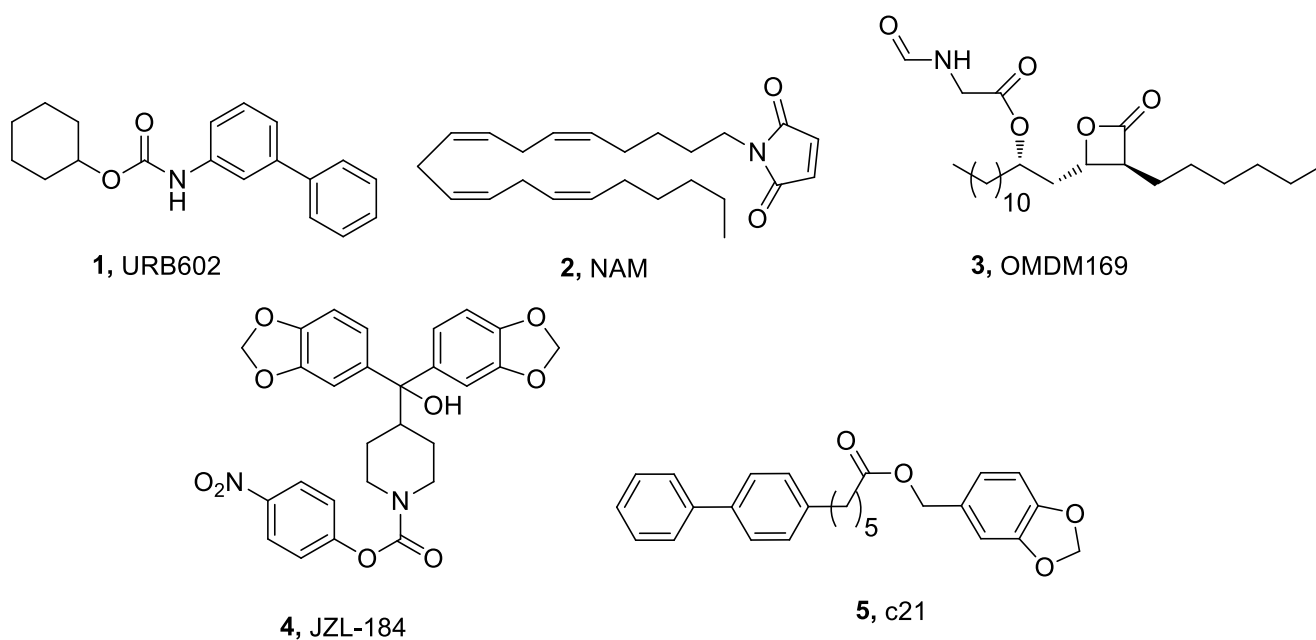


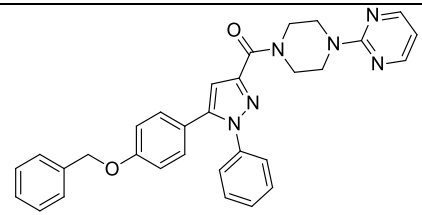
Figure 1. Representative MAGL inhibitors.

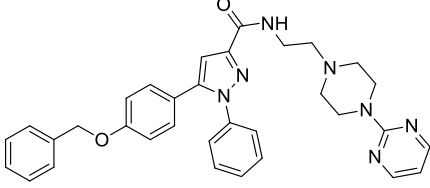
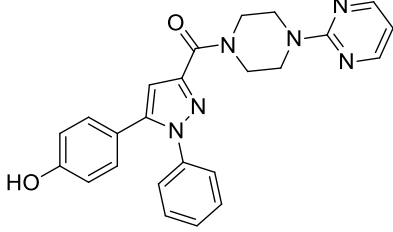
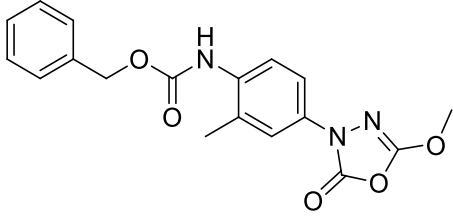
In the present study, we report the development of a diphenylpyrazole series as a new class of MAGL reversible inhibitors.

RESULTS AND DISCUSSION

From the analysis of the main available data concerning MAGL reversible inhibition,³⁴⁻³⁶ some pharmacophoric elements seem to be important for inhibitory activity: *a*) a carbonyl group able to interact into the oxyanion hole of the enzyme, *b*) an aromatic portion comprising also an heterocyclic nucleus, involved in van der Waals interactions in a closed hydrophobic region of the binding site (red region of Figure S1) and *c*) a second aromatic portion which interacts in the open large hydrophobic cavity of MAGL (green region of Figure S1). Following this binding analysis, we hypothesized that the 1,5-diphenylpyrazole scaffold, properly substituted with a carbonyl group and different fragments, could represent the starting point for the identification of new reversible MAGL inhibitors. Following these indications, we synthesized three different diphenylpyrazole derivatives (**6-8**, Table 1) characterized by different substituents. The compounds were thus tested for their MAGL inhibition activity together with the **CAY10499** derivative,³⁷ which was used as a reference compound. As shown in Table 1, the (5-(4-hydroxyphenyl)-1-phenyl-1*H*-pyrazol-3-yl)(4-(pyrimidin-2-yl)piperazin-1-yl)methanone (**8**) showed an appreciable activity with an IC₅₀ value of 6.8 μM, whereas the other two compounds were inactive.

Table 1. MAGL inhibitory activities of diphenylpyrazole derivatives.

compd	Structure	IC ₅₀ (μM)
6		>> 200

7		>> 200
8		6.8 ± 0.4
CAY10499		0.14 ± 0.02

As shown in Figure 2, the docking results for this compound highlight the presence of two H-bonds between the carbonyl oxygen of the compound and the nitrogen backbone of A51 and M123 in the oxyanion hole. The piperazinympyrimidine fragment is inserted into the closed hydrophobic region of the binding site and shows lipophilic interactions with I179, L184, V270 and a π - π interaction with Y194. The *N*-phenyl ring shows lipophilic interactions with L148, A151, L213 and L241, whereas the 5-phenol ring shows lipophilic interactions with L205 and a weak H-bond with S176.

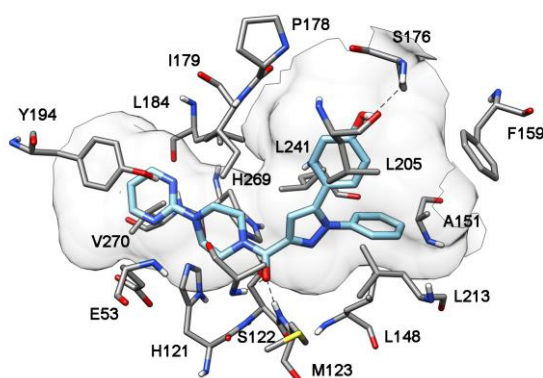
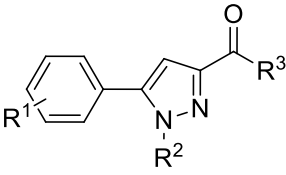
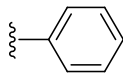
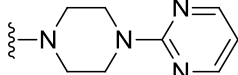
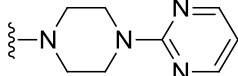
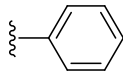
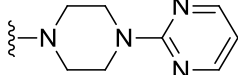
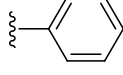
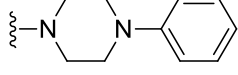
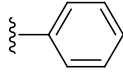
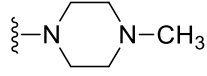
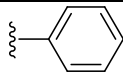
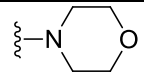
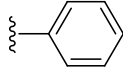
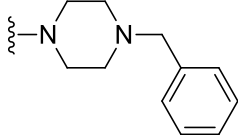
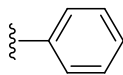
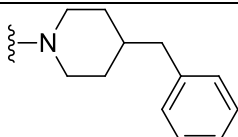
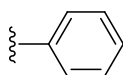
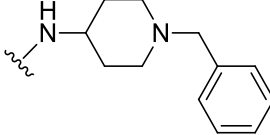
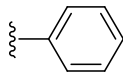
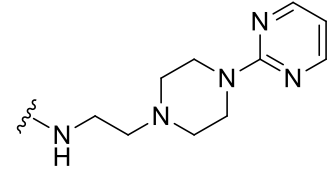


Figure 2. Docking of compound **8** into MAGL.

Using this compound as a starting hit, a first round of structural investigation has been carried out by maintaining the central pyrazole core fixed and varying: 1) the substituent present on the nitrogen atom (phenyl or methyl group) of the pyrazole ring (R^2 , Table 2); 2) the portion linked to the carbonyl group in position 3 of the pyrazole ring (R^3 , Table 2) and 3) the position of the hydroxyl group of the phenolic ring in position 5 (R^1 , Table 2). As shown in Table 2, the substitution of the 1-phenyl ring with a methyl group determined an important decrease of activity (compound **9**) compared to **8**, as well as the shift of the *p*-hydroxy group to the *meta* position (compound **10**). The replacement of the pyrimidine with a phenyl ring determined a slight increase of activity (**11**, $IC_{50} = 4.7 \mu M$), but when a benzyl group was inserted in place of the phenyl the activity was about two-fold lower (**14**, $IC_{50} = 12 \mu M$). When pyrimidine was replaced with a methyl group (**12**) or the entire piperazinyipyrimidine fragment with a morpholine ring (**13**) a ten-fold decrease of activity was observed. Conversely, the best result was achieved by the replacement of the piperazinyipyrimidine with the 4-benzylpiperidine, which led to a 3.5 fold increase of the activity (**15**, $IC_{50} = 2.0 \mu M$). Finally, the replacement of the 4-benzylpiperidine with larger dimension groups such as the 1-benzylpiperidin-4-amine of compound **16** and the 2-(4-(pyrimidin-2-yl)piperazin-1-yl)ethanamine of compound **17** led to a completely loss of activity.

Table 2. MAGL inhibitory activities of **8** derivatives.

				
compd	R^1	R^2	R^3	IC_{50} (μM)

8	4-OH			6.8 ± 0.4
9	4-OH	-CH ₃		132 ± 20
10	3-OH			48 ± 2
11	4-OH			4.7 ± 0.1
12	4-OH			71 ± 3
13	4-OH			61 ± 15
14	4-OH			12 ± 1
15	4-OH			2.0 ± 0.1
16	4-OH			$\gg 200$
17	4-OH			$\gg 200$

As shown in Figure 3, with respect to the piperazinympyrimidine of derivative **8**, the 4-benzylpiperidine of **15** is inserted deeper inside the closed hydrophobic region of the binding site and shows stronger lipophilic interactions with L184, V270 and the π - π interaction with Y194. This different disposition determines also a slight different orientation of the 5-(4-hydroxyphenyl)-1-phenyl-1*H*-pyrazole fragment with the formation of an H-bond between the hydroxyl group and the oxygen backbone of P178.

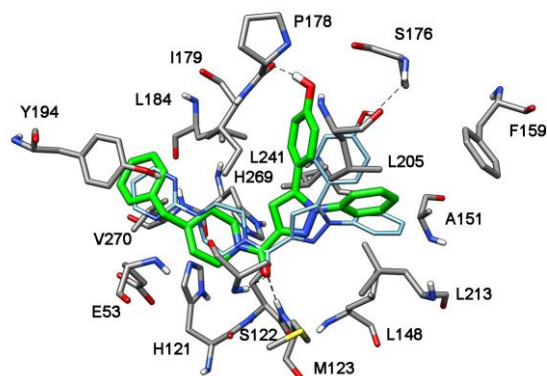
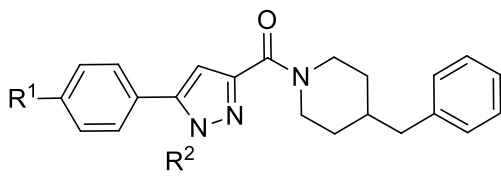
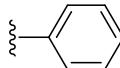
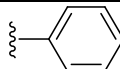
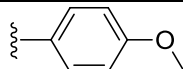
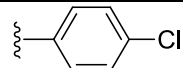
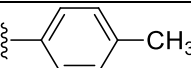
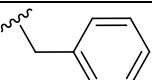
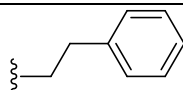
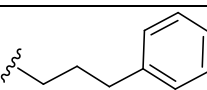
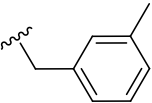
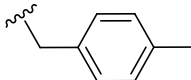


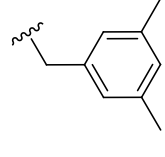
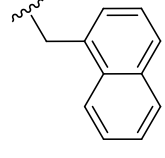
Figure 3. Docking of compound **15** (green) into MAGL. Compound **8** (cyan) is displayed as a reference compound.

In order to verify the role of the *p*-hydroxyl in the binding process, this group was removed or replaced with a chlorine atom. As shown in Table 3, in both cases (compounds **19** and **18**), the compounds showed a decrease of MAGL inhibitory activity (IC_{50} value of 13 and 11 μ M, respectively), supporting the possible attractive interaction of the *p*-hydroxy group with the enzyme, as suggested by modeling studies. The comparison between the disposition of compounds **8** and **15** suggests that the phenyl ring of **15** bound to the nitrogen atom in position 1 of the pyrazole ring appears to be shifted towards the central region of the open binding cavity and could have weaker lipophilic interactions with L148, A151 and L241, when compared to the phenyl ring of analogue **8**. On these bases, the phenyl ring of **15** was substituted with different groups, such as the *p*-methoxy (**20**), *p*-chloro (**21**) and *p*-methyl (**22**) and with different aromatic portions such as the benzyl (**23**), phenylethyl (**24**) and phenylpropyl (**25**) fragments. The enzymatic assays revealed that the introduction of the benzyl group such as in compound **23** determined the highest increase of inhibitory activity ($IC_{50} = 0.81 \mu$ M, Table 3). Then, in order to maximize the lipophilic interactions of this fragment, methyl groups in *para* and *meta* position of the benzyl moiety were introduced (**26**, **27** and **28**). Finally, a naphthylmethyl group (**29**) was inserted in the place of the benzyl group. As shown in

Table 3, the *meta*-methyl substitution of the benzyl ring determined a further slight improvement of the MAGL inhibitory activity, with a resulting IC₅₀ of 0.51 μM (compound **26**).

Table 3. MAGL inhibitory activities of 4-benzylpiperidines (compound **15** derivatives).

			
compd	R ¹	R ²	IC ₅₀ (μM)
18	Cl		11 ± 3
19	H		13 ± 1
20	OH		3.2 ± 0.1
21	OH		1.4 ± 0.2
22	OH		1.5 ± 0.1
23	OH		0.81 ± 0.02
24	OH		4.3 ± 0.4
25	OH		1.6 ± 0.1
26	OH		0.51 ± 0.03
27	OH		1.1 ± 0.1

28	OH		1.4 ± 0.1
29	OH		1.6 ± 0.3

As shown in Figure 4, the binding disposition of compound **26** is very similar to that observed for **15**, maintaining the lipophilic interactions of the 4-benzylpiperidine with L184, V270 and the π - π interaction with Y194, the interaction of the carbonyl group in the oxyanion hole and the H-bond between the *p*-hydroxyl group and the oxygen backbone of P178. Differently from **15**, the *m*-methylbenzyl fragment points towards the surface of the binding site and shows stronger lipophilic interactions with in particular A151 and L241.

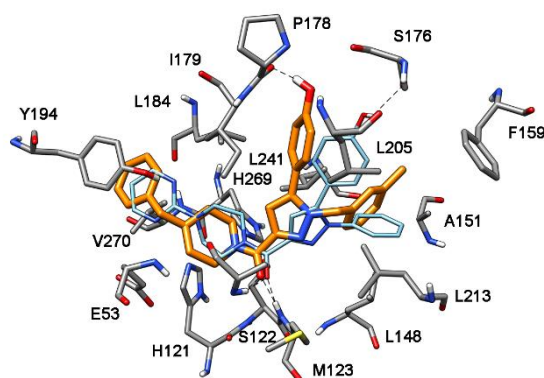


Figure 4. Docking of compound **26** (orange) into MAGL. Compound **8** (cyan) is displayed as a reference compound.

With the aim of evaluating the reversible or irreversible mechanism of inhibition, the effects of dilution and preincubation on the inhibitory ability of compound **26** were evaluated. In the dilution experiments, in case of an irreversible inhibition, the potency should not decrease after dilution.

Differently, in case of a reversible inhibition, the potency level should be substantially reduced after dilution.³⁸ In our experiment, the inhibition produced by preincubation with a 20 μM concentration of **26** was measured after a 40X dilution and compared to the potency observed by a 20 μM and a 0.5 μM of compound **26**. As shown in Figure 5A, **26** showed a reversible inhibition mechanism, as the inhibition produced by 0.5 μM of the compound was similar to that of 40X dilution, and was different to that produced by the compound at a concentration of 20 μM . As a second test, the activity of **26** was assayed at different preincubation times of the compound with MAGL. In this assay, the compound is incubated with the enzyme 30 and 60 minutes before the addition of the substrate and the observed IC_{50} is then compared with that obtained without a preincubation of the compound with the enzyme. An irreversible inhibitor will show a higher potency with a higher incubation time whereas a reversible inhibitor will show a constant inhibition potency independent from the incubation time. As shown in Figure 5B, this assay confirmed the reversible property of **26**, as it did not show any significant increase in inhibition potency with different incubation times.

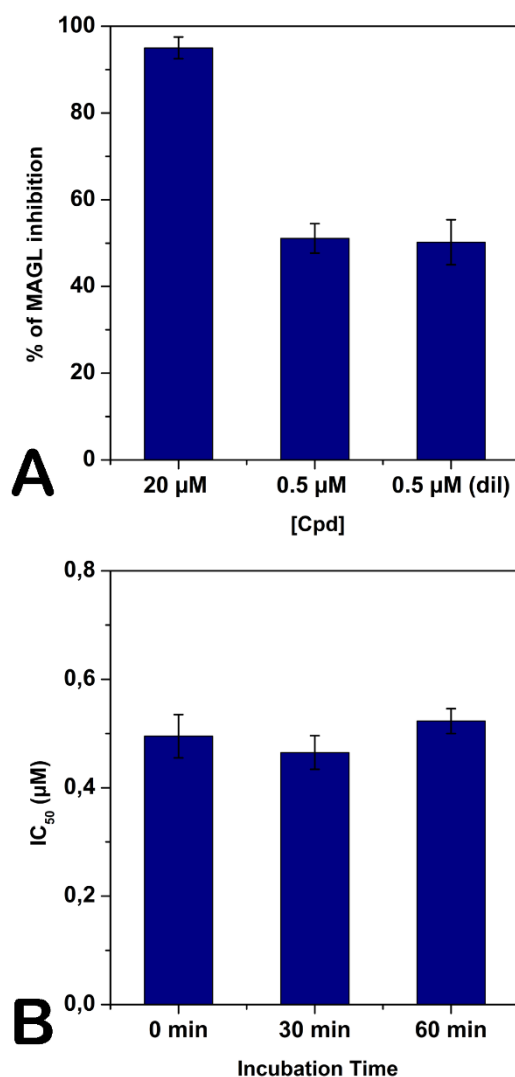


Figure 5. Compound **26**-MAGL inhibition analysis. A) Dilution assay: the first two columns indicate the inhibition percentage of compound **26** at a concentration of 20 μM and 0.5 μM . The third column indicates the inhibition percentage of compound **26** after dilution (final concentration = 0.5 μM). B) IC₅₀ (μM) values of **26** at different preincubation times with MAGL (0 min, 30 min and 60 min).

Once confirmed the reversible mechanism of compound **26**, its inhibition mode was then determined by evaluating Michaelis-Menten kinetics with various inhibitor concentrations. The dataset was plotted as substrate concentration *versus* MAGL activity and evaluated by using the mixed-model inhibition fit of GraphPad Prism 5.0, thus including competitive, uncompetitive, and noncompetitive inhibition terms. This analysis produces the V_{max} , K_m , K_i and the α value, a parameter consisting of a

positive number (α is always greater than zero) that can be used as an indicator of the mechanism of inhibition. In fact, when α is smaller than one, then the mixed model becomes nearly identical to an uncompetitive model; when it is equal to one, then the mixed-model is identical to a noncompetitive inhibition; finally, when α has a very large value, then the mixed-model becomes identical to a competitive inhibition. As shown in Figure 6, the Michaelis-Menten-type curve resulted in K_m values of 0.21 ± 0.07 mM, V_{max} value of $42 \pm 1 \mu\text{mol}\cdot(\text{min}^{-1}\text{mg}^{-1})$, a K_i value for **26** of 412 ± 19 nM and an α value greater than 100000, thus supporting a competitive behavior for the selected compound.

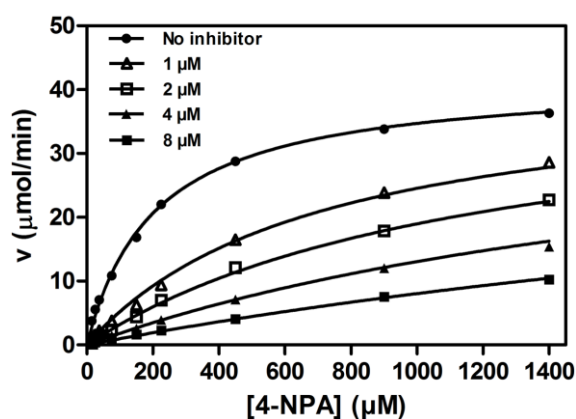


Figure 6. Inhibition of the activity of MAGL and competitive nature of compound **26**.

Selectivity analysis. With the aim of evaluating the selectivity of compound **26** versus the other major endocannabinoid degrading enzymes, its activities against FAAH, ABHD6 and ABHD12 were tested. As shown in Table 4, compound **26** did not show any significant inhibition of FAAH and ABHD12 at the concentration of 10 μM (7% and 32% of inhibition for FAAH and ABHD12, respectively), while ABHD6 was actually inhibited with an IC_{50} value of $7.1 \pm 2.3 \mu\text{M}$. Thus compound **26** behaves as MAGL inhibitor showing good selectivity over FAAH, ABHD6 and ABHD12 (see the Experimental section for details). Finally, since the diarylpyrazoles are a well-known class of cannabinoid receptor ligands,³⁹ the possible affinities of compound **26** for the cannabinoid receptors

CB₁ and CB₂ were also evaluated. As reported in Table 4 this compound did not show a significant binding to any of the two cannabinoid receptor subtypes.

Table 4. Biological activity of compound **26** on the major components of the endocannabinoid system. Effects on FAAH, ABHD6, ABHD12, CB₁ and CB₂ receptors are expressed as IC₅₀ value (mean ± SD, μM). In bracket the % enzymatic inhibition (FAAH and ABHD12) or receptor binding (CB₁ and CB₂ receptors) at 10 μM is reported.

compd	FAAH	ABHD6	ABHD12	CB ₁ binding	CB ₂ binding
26	> 10 (7%)	7.1 ± 2.3	> 10 (32%)	> 10 (22%)	> 10 (35%)

Antiproliferative assays. Compound **26** was further tested in *in vitro* experiments to evaluate its antiproliferative potency against cancer cells, together with compound **CAY10499**, which was used as the reference compound. As suggested by literature data, MAGL is an optimal candidate target for ovarian cancer.²⁸ Western blot analysis has recently highlighted that MAGL is overexpressed in OVCAR3 and CAOV3 compared to OVSAHO and COV318 cell lines.³⁴ These cell lines were selected since they represent more closely high-grade serous ovarian cancer (HG-SOC),⁴⁰ a fatal tumor. At the molecular level, all cell lines are mutated in the TP53 gene, BRCA2 gene (OVSAHO) or the cell cycle pathway (OVSAHO, COV318, OVCAR3), which are common events in HG-SOC. Therefore, the antiproliferative activity of the two compounds was tested against these four cell lines, together with the noncancerous human fibroblast lung cells (MRC5). As shown in Table 5, compound **26** caused a good inhibition of cell viability, with IC₅₀ values of 12 and 11 μM in the OVCAR3 and CAOV3 cell lines, respectively, whereas it proved to be about 7-fold less potent against ovarian cancer cells that do not overexpress MAGL, such as OVSAHO and COV318 cells. Furthermore, **26** proved to be inactive also against noncancerous human fibroblast lung cells (MRC5, IC₅₀ > 100 μM). The covalent reference inhibitor **CAY10499** showed inhibition of cell viability in all the four ovarian

cancer cell lines, with IC₅₀ values ranging from 23 to 77 μM without any significant discrimination between the two MAGL-overexpressing cell lines OVCAR3 and CAOV3 and the other two lines, OVSAHO and COV318.

Table 5. Cell growth inhibitory activities (IC₅₀) of compounds **24** and **CAY10499**.

	IC ₅₀ values (μM)				
	OVSAHO	OVCAR3	COV318	CAOV3	MRC5
26	90 ± 6	12 ± 2	78 ± 6	11 ± 1	> 100
CAY10499	23 ± 2	43 ± 6	59 ± 4	77 ± 7	> 100

Antinociceptive effects of 26 in animal model of neuropathic pain. The effect of **26** was evaluated in a mouse model of nociceptive behavior caused by the chemotherapeutic agent, oxaliplatin (cold plate test). The pain threshold measurements of oxaliplatin-treated animals are shown in Figure 7. The cold plate test allows to evaluate the response to a thermal non noxious stimulus defined as allodynia-like. On day 15, oxaliplatin decreased the licking latency to 10.0 ± 0.5 s in comparison to control mice (17.6 ± 0.4 s). A single treatment p.o. with **26** relieved pain dose-dependently. The lower dose of 10 mg/kg induced a significant effect 30 min after the administration. At 30 mg/kg the compound reduced oxaliplatin-induced neuropathic pain 30 and 45 min after treatment and in particular, after 30 min it increased pain threshold to a value similar to that shown by control animals (vehicle + vehicle).

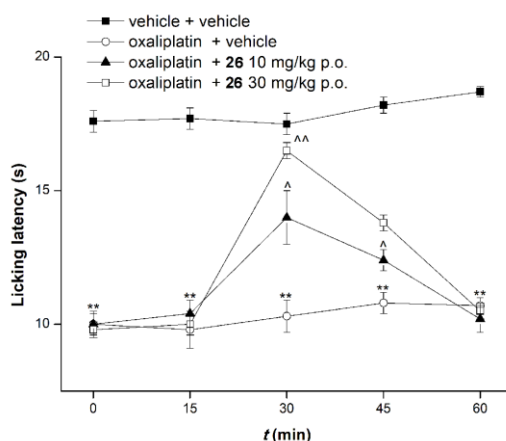


Figure 7. Effect of **26** on oxaliplatin-induced neuropathic pain. Oxaliplatin (2.4 mg/kg) was dissolved in 5% glucose solution and administered i.p. on days 1-2, 5-9, 12-14. On day 15, **26** (10 and 30 mg/kg) was suspended in carboxymethylcellulose (CMC) and p.o. administered. Pain-related behavior (i.e. lifting and licking of the hind paw) was observed by the cold plate test and the time (s) of the first sign was recorded. **P<0.01 vs Vehicle + Vehicle treated animals; ^P<0.05 and ^^P<0.01 vs oxaliplatin + Vehicle group. Each value represents the mean of 10 mice performed in 2 different experimental sets.

In order to test the effects of the compound after repeated treatments, **26** (30 mg/kg, p.o.) was co-administered with oxaliplatin from day 1 to day 14 following the same protocol. Pain threshold was evaluated by cold plate test on days 7 and 15, 24 h after the last administration. As shown in Figure 8 (upper panel), oxaliplatin induced a significant hypersensitivity both the first and the second week. Compound **26** significantly reduced cold allodynia on day 7 as well as on day 15. The effect progressively increased overtime. On day 15, 24 h after the last administration, mice treated with **26** showed a complete pain relief. These results highlight: i) the long lasting efficacy of the compound after repeated treatments, ii) the increasing activity during treatment, suggesting protective properties against oxaliplatin neurotoxicity, iii) the complete lack of tolerance development.

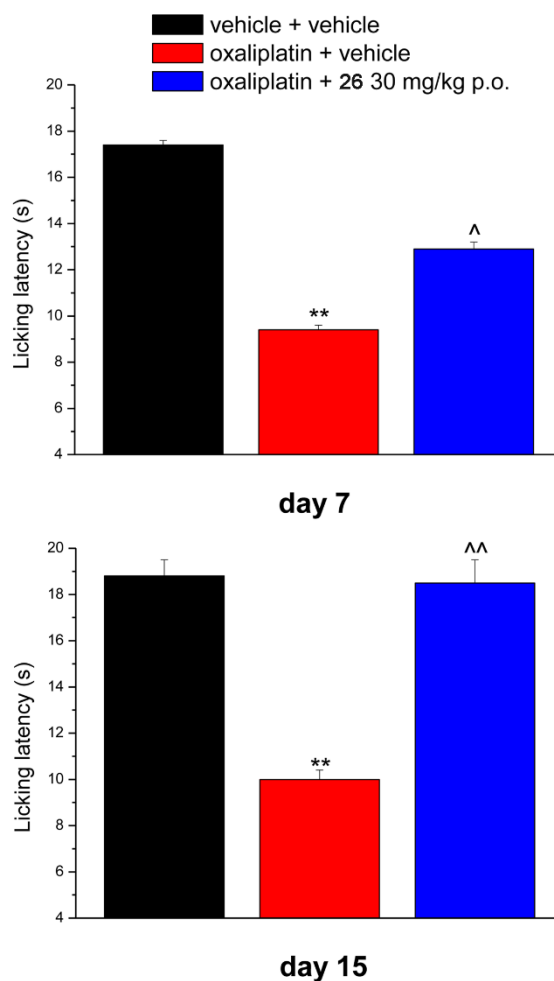


Figure 8. Anti-neuropathic pain activity of **26** after subchronic treatment. Oxaliplatin (2.4 mg/kg) was dissolved in 5% glucose solution and administered i.p. on days 1-2, 5-9, 12-14. **26** (30 mg/kg) was suspended in carboxymethylcellulose (CMC) and administered p.o. using the same protocol as that for oxaliplatin alone. The cold plate test was performed 24 h after the last administration on days 7 and 15 observing the pain-related behavior (i.e. lifting and licking of the hind paw). **P<0.01 vs vehicle + vehicle treated animals; ^P<0.05 and ^^P<0.01 vs oxaliplatin + vehicle group. Each value represents the mean of 10 mice performed in 2 different experimental sets.

We also quantified by LC-MS/MS the amount of 2-AG, AEA, arachidonic acid, prostaglandin-E2 (PGE2) and prostaglandin-D2 (PGD2) in brain and spinal cord after 15 days of treatment. Animals treated with oxaliplatin and compound **26** did not show any significant difference in 2-AG levels as

compared to oxaliplatin-treated mice (see Figure S2). Previous studies reported that covalent MAGL inhibitors exert significant anti-allodynic effects in different mouse models of neuropathic pain.⁴¹⁻⁴⁴ However, in these animal models MAGL inhibition exerted opposite effects on the modulation of 2-AG concentrations in brain, spinal cord and dorsal root ganglia (DRGs). For example, Kinsey et al. reported a marked increase of 2-AG levels in brain and spinal cord of mice treated with a single injection of JZL184 (16 mg/kg, ip) 14 days after chronic constriction injury (CCI) surgery.⁴¹ On the contrary, Khasabova et al. reported no significant change in 2-AG levels in brain and spinal cord after 7 days of treatment with cisplatin and JZL184 (10 µg, subcutaneous injection).⁴⁵ In the same study, JZL184 was able to recover the cisplatin-induced reduction of 2-AG level in DRGs. Wilkerson et al. showed that suprathreshold dose of MJN110 (0.1432 mg/kg, ip) could only marginally increase 2-AG level in the spinal cord of mice subjected to CCI surgery while not affecting 2-AG level in the brain.⁴⁴ Our data showed that compound **26** did not increase 2-AG levels in brain and spinal cord of mice treated for 15 days, despite inducing significant anti-allodynic effects. This may be due to a mild and specific increase of 2-AG concentrations in specific brain or spine regions. Alternatively, compound **26** may exhibit only a negligible penetration or activity in the central nervous system. Previous studies showed that the anti-allodynic effect of FAAH and MAGL inhibitors is associated with the modulation of AEA and 2-AG levels in DRGs.^{45, 46} Thus, we may speculate that the anti-allodynic effect induced by compound **26** could be associated with the modulation of 2-AG levels in the peripheral nervous system (i.e. DRGs). In agreement with this hypothesis, it was shown that the disposition of cisplatin is limited to peripheral tissues and DRGs were the most vulnerable neural structure.⁴⁷ However, we cannot exclude the possibility that the *in vivo* effects showed by compound **26** may also be dependent by alternative mechanisms beyond MAGL inhibition.

Chemistry. The diphenylpyrazole compounds **6-29** were prepared as shown in Scheme 1. Claisen condensation of commercially available acetophenones **28b-d** or 4'-benzyloxyacetophenone **28a**⁴⁸ (for the preparation of compounds **6** and **7**) with diethyl oxalate afforded the corresponding

CONCLUSIONS

In the present work we have reported a new class of MAGL reversible inhibitors. Starting from (5-(4-hydroxyphenyl)-1-phenyl-1H-pyrazol-3-yl)(4-(pyrimidin-2-yl)piperazin-1-yl)methanone (**8**) a structural optimization has been performed leading to the identification of compound **26**, which displayed a high MAGL inhibition activity with a K_i of 412 nM. This reversible inhibitor was then tested in cell-based assays where it showed promising cell growth inhibitory activities in an antiproliferative assay in the OVCAR-3 and CAOV3 cell lines that overexpress MAGL. Furthermore, oral administration of **26** dose dependently reversed the lowering of the threshold to cold stimuli (cold plate test) induced by oxaliplatin, indicating its efficacy in the treatment of neuropathic pain. The efficacy increased after repeated administration suggesting a possible protective effect in the absence of tolerance development, even if evidences about the *in vivo* actual inhibition of MAGL after administration of the compound are needed. Taken together these results suggest that these new compounds could open new perspectives for developing novel reversible MAGL inhibitors.

EXPERIMENTAL SECTION

Pan Assay Interference Compounds (PAINS) analysis. In order to exclude the possibility that the herein reported class of compounds could act as artifacts or promiscuous bioactive molecules, a PAINS analysis for the most active compound (**26**) was carried out.⁵¹

PAINS substructural features screening. As reported by Baell and Holloway there is a number of substructural features which could help to identify compounds that appear as PAINS in many biochemical high throughput screens.⁵² The corresponding filters have been included in the Filter-it™ software and compound **26** was thus filtered by using this program. The result highlighted that this compound did not possess any of the substructural features shared by the most common PAINS.

Interference analysis. Some PAINS are associated with color that could interfere photometrically with the assay. In order to avoid this possibility for each compound concentration a blank analysis

was carried out, and the final absorbance values were obtained subtracting the absorbance determined by the presence of all the components except the enzyme in the same conditions.

Aggregation analysis. In order to exclude possible aggregation behaviors, all the enzymatic assays were carried out in the presence of bovine serum albumin (BSA) 0.1 mg/ml.

Thiol reactive analysis. In some cases, PAINS properties could be caused by a covalent interaction between a ligand and cysteines of multiple proteins.⁵³ In order to investigate this possibility, the inhibition activity of **26** against MAGL was tested in the presence of the thiol-containing agent 1,4-dithio-DL-threitol (DTT).⁵⁴ This assay suggested that the inhibition potency of **26** was not affected by the presence of DTT, as it showed an $IC_{50} = 0.50 \pm 0.04 \mu\text{M}$ when assayed with 100 μM DTT, thus excluding the interaction of this compound with the cysteine residues of the MAGL enzyme.

Selectivity testing. As reported by Dahlin and Walters⁵⁵ a selectivity analysis is another test that would contribute to highlight most PAINS. As reported in the text we measured the activity of compound **26** against FAAH, ABHD6 and ABHD12 resulting in a good MAGL selectivity.

Orthogonal assay. The application of a different readout method for measuring the activity against the target is another step that contribute to elucidate the PAINS properties. For this reason the activity of **26** against MAGL was also tested by using an HPLC/UV assay.⁵⁶ An aliquot of stock solutions of MAGL was diluted 1:125 with Tris buffer (pH = 7.2; 10 mM, containing 1.0 mM EDTA) to obtain the working solutions of MAGL at 1.6 ng/ μl . The stock and working solutions were stored at -20°C . In a 0.5 ml spin tube containing 75 μl of Tris buffer (pH = 7.2; 10 mM containing 1.0 mM EDTA), 5 μl of working solution MAGL (8 ng), 5 μl inhibitor (or solvent as control) and 5 μl of a solution of 4-nitrophenylacetate (4-NPA) substrate in absolute ethanol (4.25 mM) were added. Samples were incubated for 10 min, then the enzymatic reaction was stopped by cooling in an ice bath for 10 min and 20 μl of the reaction mixture were taken and analyzed by HPLC. Shimadzu Prominence HPLC system was used to quantify 4-nitrophenol formed after enzymatic hydrolysis of 4-NPA by using a

diode-array detector at operation wavelength of 310 nm. Separation of compounds was carried out on a Kinetex EVO C18 column (5 μm , 150 mm \times 4.6 mm, Phenomenex, Inc.). The mobile phase, delivered at a flow rate of 1.0 ml/min and consisted of methanol and ammonium acetate buffer (pH 4.0; 10 mM) (53:47, v/v). The sample injection volume was 20 μl . Data were monitored and analyzed using chromatography Software LabSolutions Lite (Shimadzu). By using this assay method, compound **26** showed an IC_{50} against MAGL of $0.39 \pm 0.05 \mu\text{M}$, thus confirming the inhibition activity measured by the colorimetric assay.

Docking Calculations. The crystal structure of human MAGL (pdb code 3PE6³⁵) was minimized using Amber14 software⁵⁷ and ff14SB force field at 300 K. The TIP3P explicit solvent model for water, was used with a 10 \AA water cap. In order to neutralize the system, sodium ions were added. Two minimization steps of were performed; in the first stage, the protein was kept fixed with a position restraint of 500 kcal/mol \AA^2 minimizing the positions of the water molecules. In the second stage, the entire system was minimized through 5000 steps of steepest descent followed by conjugate gradient (CG) until a convergence of 0.05 kcal/ $\text{\AA}\cdot\text{mol}$. The ligands were built using Maestro⁵⁸ and were minimized by means of MacroModel⁵⁹ in a water environment using the CG method using the MMFFs force field. Docking analysis was performed by means of the AUTODOCK 4.0 program;⁶⁰ Autodock Tools⁶¹ was used in order to identify the torsion angles in the ligands, add the solvent model and assign the Kollman atomic charges to the protein. The ligand charge was calculated using the Gasteiger method. The ZYH reference inhibitor was used in order to identify the binding site; a grid of 82, 40, and 30 points in the x, y, and z directions was constructed centered on the center of the mass of this compound. A grid spacing of 0.375 \AA and a distance-dependent function of the dielectric constant were used for the energetic map calculations. Using the Lamarckian Genetic Algorithm, the docked compounds were subjected to 100 runs of the Autodock search, using 500000 steps of energy evaluation and the default values of the other parameters. Cluster analysis was performed on the results using an RMS tolerance of 2.0 \AA .

MAGL inhibition assay. Human recombinant MAGL, **CAY10499** and 4-NPA substrate were from Cayman Chemical. The enzymatic reaction was carried out at room temperature (final volume of 200 μ L in 10 mM Tris buffer, pH 7.2, containing 1 mM EDTA and 0.1 mg/ml BSA). A total of 150 μ L of 4-NPA 133.3 μ M (final concentration = 100 μ M) was added to 10 μ L of DMSO containing the appropriate amount of compound and the reaction was initiated by the addition of 40 μ L of MAGL (11 ng/well). The final concentration of the analyzed compounds ranged for **CAY10499** from 10 to 0.00001 μ M and for the other compounds from 200 to 0.0128 μ M. After the reaction had proceeded for 30 min, absorbance values were then measured by using a Victor X3 Microplates Reader (PerkinElmer®) at 405 nm.³⁷ The assay was generated in 96-well microtiter plates. Two reactions were also run: one reaction containing no compounds and the second one containing neither inhibitor nor enzyme. IC₅₀ values were derived from experimental data using the Sigmoidal dose–response fitting of GraphPad Prism software. To remove possible false positive results, for each compound concentration a blank analysis was carried out, and the final absorbance results were obtained deducting the absorbance produced by the presence of all the components except MAGL in the same conditions. In the enzyme kinetics experiments, compound was tested in the presence of scalar concentrations of 4-NPA. It was added in scalar amounts (concentration range = 1–8 μ M) to a reaction mixture containing Tris buffer and scalar concentrations of 4-NPA (15–1400 μ M). Finally, MAGL solution was added (11 ng/well). The MAGL activity was measured by recording the increase in 4-nitrophenol absorbance using the Victor X3 Microplates Reader (PerkinElmer®). The experimental data were analyzed by non-linear regression analysis with GraphPad Prism software, using a second order polynomial regression analysis, and by applying the mixed-model inhibition fit.

FAAH inhibition assay. Human recombinant FAAH and AMC arachidonoylamide substrate were from Cayman Chemical. The FAAH reaction was conducted at room temperature (final volume of 200 μ L in 125 mM Tris buffer, pH 9.0, containing 1 mM EDTA and 0.1 mg/ml BSA). A total of 150 μ L of AMC arachidonoylamide 13.3 μ M (final concentration = 10 μ M) was added to 10 μ L of DMSO containing the appropriate amount of compound. The reaction was initiated by the addition of 40 μ L

of FAAH (0.9 $\mu\text{g}/\text{well}$) in such a way that the assay was linear over 30 min. The final concentration of the analyzed compounds ranged for from 200 to 0.0128 μM . After the reaction had proceeded for 30 min, fluorescence values were then measured by using a Victor X3 PerkinElmer instrument at an excitation wavelength of 340 nm and an emission of 460 nm. As for MAGL assay, two reactions were also run: one reaction containing no compounds and the second one containing neither inhibitor nor enzyme. IC_{50} values were derived from experimental data using the Sigmoidal dose–response fitting of GraphPad Prism software. To remove possible false positive results, for each compound concentration a blank analysis was carried out, and the final fluorescence results were obtained deducting the fluorescence produced by the presence of all the components except FAAH in the same conditions. Furthermore, compound **26** was also tested for FAAH inhibition using mouse brain homogenate as previously reported.⁸

CB₁ and CB₂ receptor binding assays. Receptor binding experiments were performed with membrane preparations as previously reported.⁶² Briefly, clean membranes expressing *hCB₁* or *hCB₂* were re-suspended in binding buffer (50 mM Tris-HCl, 2.5 mM EDTA, 5 mM MgCl₂, 0.5%¹ fatty acid-free bovine serum albumin (BSA), pH 7.4) and incubated with vehicle or compounds and 0.5 nM of [³H]CP55,940 for 90 min at 30 °C. Non-specific binding was determined in the presence of 10 μM of WIN55,512. After incubation, membranes were filtered through a pre-soaked 96-well microplate bonded with GF/B filters under vacuum and washed twelve times with 150 μL of ice-cold binding buffer. The radioactivity was measured and the results expressed as [³H]CP55,940 binding.

ABHD6 and ABHD12 inhibition assay. ABHDs activity assays were performed as previously described.⁸ The *hABHD6* and *hABHD12* activity was determined using cell homogenates from *hABHD6* and *hABHD12* stably transfected HEK293 cells. Compound was pre-incubated with 40 μg of cell homogenate for 30 min at 37 °C in assay buffer (Tris 1 mM, EDTA 10 mM plus 0.1% BSA, pH= 7.6). DMSO was used as vehicle control and WWL70 10 μM or THL 20 μM as positive controls. Then, 10 μM of 2-OG was added and incubated for 5 min at 37 °C. The reaction was stopped by the addition of 400 μL of ice-cold CHCl₃:MeOH (1:1). The samples were vortexed and centrifuged

(16000 x g, 10 min, 4 °C). Aliquots (200 µL) of the aqueous phase were assayed for tritium content by liquid scintillation spectroscopy. Blank values were recovered from tubes containing no enzyme. Basal 2-OG hydrolysis occurring in non-transfected HEK293 cells was subtracted.

Cell viability assay. OVSAHO, OVCAR3, COV318, CAOV3 and MRC5 (from ATCC) were maintained at 37 °C in a humidified atmosphere containing 5% CO₂ accordingly to the supplier. Normal (1.5×10^4) and tumor (5×10^2) cells were plated in 96-well culture plates. The day after seeding, vehicle or compounds were added at different concentrations to the medium. Compounds were added to the cell culture at a concentration ranging from 100 to 0.01 µM. Cell viability was measured after 96 h according to the supplier (Promega, G7571) with a Tecan F200 instrument. IC₅₀ values were calculated from logistical dose response curves. Averages were obtained from three independent experiments, and error bars are standard deviations (n = 3).

Animals. Male CD-1 albino mice (Envigo, Varese, Italy) weighing approximately 22–25 g at the beginning of the experimental procedure, were used. Animals were housed in CeSAL (Centro Stabulazione Animali da Laboratorio, University of Florence) and used at least 1 week after their arrival. Ten mice were housed per cage (size 26 × 41 cm); animals were fed a standard laboratory diet and tap water *ad libitum*, and kept at 23 ± 1 °C with a 12 h light/dark cycle, light at 7 a.m. All animal manipulations were carried out according to the European Community guidelines for animal care (DL 116/92), application of the European Communities Council Directive of 24 November 1986 (86/609/EEC). The ethical policy of the University of Florence complies with the Guide for the Care and Use of Laboratory Animals of the US National Institutes of Health (NIH Publication No. 85-23, revised 1996; University of Florence assurance number: A5278-01). Formal approval to conduct the experiments described was obtained from the Animal Subjects Review Board of the University of Florence. Experiments involving animals have been reported according to ARRIVE guidelines. All efforts were made to minimize animal suffering and to reduce the number of animals used.

Oxaliplatin-induced neuropathic pain model. Mice treated with oxaliplatin (2.4 mg/kg) were administered i.p. on days 1-2, 5-9, 12-14 (10 i.p. injections)^{63, 64} oxaliplatin was dissolved in 5%

glucose solution. Control animals received an equivalent volume of vehicle. Behavioral tests were performed on day 15.

Cold plate test. The animals were placed in a stainless steel box (12 cm × 20 cm × 10 cm) with a cold plate as floor. The temperature of the cold plate was kept constant at 4 °C ± 1 °C. Pain-related behavior (licking of the hind paw) was observed and the time (seconds) of the first sign was recorded. The cut-off time of the latency of paw lifting or licking was set at 60 seconds.⁶⁵

LC-MS/MS quantification of endocannabinoids and other metabolites. The amount of 2-AG, AEA, arachidonic acid (AA), prostaglandin-E2 (PGE2) and prostaglandin-D2 (PGD2) were measured by LC-MS/MS in brain and spinal cord of mice treated for treated for 14 days with oxaliplatin (2.4 mg/kg, i.p.) and compound **26** (30 mg/kg, p.o.) or vehicle. At day 15, animals were sacrificed by decapitation 1 h after the last dose and brain and spinal cord were collected, quickly washed in PBS and snap-frozen. Tissue extraction and LC-MS/MS conditions were performed as previously described.⁸

Statistical analysis. Behavioral measurements were performed on 10 mice for each treatment carried out in 2 different experimental sets. Results were expressed as mean ± S.E.M. The analysis of variance of behavioral data was performed by one way ANOVA, a Bonferroni's significant difference procedure was used as post-hoc comparison. *P* values of less than 0.05 or 0.01 were considered significant. Investigators were blind to all experimental procedures. Data were analyzed using the “Origin 9” software (OriginLab, Northampton, USA).

General Procedures and Materials. ¹H NMR data were recorded with a Varian VXR 200 spectrometer or a Varian Mercury Plus 400 spectrometers. Chemical shifts (δ) are reported in parts per million, and J values are given in Hertz. Positive ion electrospray ionization (ESI) mass spectra were recorded on a double-focusing Finnigan MAT 95 instrument with BE geometry. Melting points (mp) were determined on a Buchi-Tottoli apparatus and are uncorrected. Chromatography was performed on Merck 230–400 mesh silica gel and a mixture of ethyl acetate and petroleum ether in different ratios as mobile phase The purity of tested compounds was determined by combustion

elemental analyses in the Microanalytical Laboratory of the Chemistry Department of the University of Ferrara with a Yanagimoto MT-5 CHN recorder elemental analyser. All tested compounds yielded data consistent with a purity of at least 95% as compared with the theoretical values. TLC was carried out using glass plates coated with silica gel 60 F254 by Merck, and compounds were visualized by UV lamp (254 nm light source). Organic solutions were dried over anhydrous Na₂SO₄. Solvents and reagents were purchased from Aldrich (Sigma-Aldrich) or Alfa Aesar (Johnson Matthey Company) and were used without further purification. HPLC analysis: all target compounds (i.e., assessed in biological assays) were $\geq 95\%$ pure by HPLC, confirmed via UV detection ($\lambda = 254$ nm). Analytical reversed-phase HPLC was conducted using a Kinetex EVO C18 column (5 μ m, 150 mm \times 4.6 mm, Phenomenex, Inc.). Compounds were dissolved in acetonitrile or methanol, and injected through a 20 μ l loop. Eluent A was water and eluent B was CH₃CN; after 5 min at 25% B, a gradient was formed from 25% to 75% of B in 5 min and held at 75% of B for 10 min; flow rate was 1 mL/min. For compound **9**, a different gradient profile of mobile phase was used: after 5 min at 10% B, a gradient was formed from 10% to 25% of B in 5 min and then from 25% to 75% of B in the following 2.5 min and held at 75% of B for 7.5 min; flow rate was 1 mL/min. The different method was used since **9** was the only target compound bearing an alkyl group (a methyl group) as R₂ substituent (Table 2), while all the other compounds possess an aromatic group in that position. The ethyl 2,4-dioxobutanoate derivatives (**29a-d**) were prepared as previously reported by our group.⁵⁰ Ethyl 1-phenyl-5-(4-hydroxyphenyl)-1*H*-pyrazole-3-carboxylate **30b**, ethyl 1-methyl-5-(4-hydroxyphenyl)-1*H*-pyrazole-3-carboxylate **30c**, ethyl 1-(4-chlorophenyl)-5-(4-hydroxyphenyl)-1*H*-pyrazole-3-carboxylate **30e**, and ethyl 1-phenyl-5-(3-hydroxyphenyl)-1*H*-pyrazole-3-carboxylate **30n** with the corresponding carboxylic acids **31b**, **31c**, **31e**, and **31n** respectively, are described in our previously published work.⁵⁰

General procedure for the synthesis of 1,5-diphenylpyrazole-3-carboxamides (6-29). To a solution of the appropriate carboxylic acid (1.14 mmol) in dry DMF (10 mL), 1-[3-(dimethylamino)-

propyl]-3-ethylcarbodiimide (EDCI, 1.70 mmol) and 1-hydroxybenzotriazole (HOBt, 1.70 mmol) were added and the reaction was stirred at room temperature for 10 min before adding the suitable amine (1.36 mmol) and the stirring continued for 16 h. The solvent was evaporated under reduced pressure and the residue was dissolved in ethyl acetate (30 mL), washed with aqueous bicarbonate (10 mL), water (10 mL) and brine (10 mL). The mixture was concentrated and purified by silica gel column chromatography using as eluent an appropriate mixture of ethyl acetate and petroleum ether.

(5-(4-(Benzyloxy)phenyl)-1-phenyl-1*H*-pyrazol-3-yl)(4-(pyrimidin-2-yl)piperazin-1-yl)methanone (6). White solid: yield 68%; mp 170 °C; ¹H NMR (200 MHz, DMSO-*d*₆): δ 8.39 (d, *J* = 4.6 Hz, 2H), 7.46-7.32 (m, 10H), 7.20(d, *J* = 8.8 Hz, 2H), 6.99 (d, *J* = 8.8 Hz, 2H), 6.89 (s, 1H), 6.67 (t, *J* = 5 Hz, 1H), 5.09 (s, 2H), 4.04 (m, 2H), 3.81 (m, 6H). MS (ESI) 517.2 [M+H]⁺. Anal. (C₃₁H₂₈N₆O₂) C, H, N. HPLC analysis: retention time = 13.884 min; peak area, 99% (254 nm).

5-(4-(Benzyloxy)phenyl)-1-phenyl-*N*-(2-(4-(pyrimidin-2-yl)piperazin-1-yl)ethyl)-1*H*-pyrazole-3-carboxamide (7). White solid: yield 60%; mp 152 °C; ¹H NMR (200 MHz, DMSO-*d*₆): δ 8.34 (d, 2H, *J* = 4.8 Hz), 8.25 (t, 1H), 7.38-7.45 (m, 10H), 7.18 (d, 2H, *J* = 8.6 Hz), 6.98 (d, 2H, *J* = 8.6 Hz), 6.92 (s, 1H), 6.64 (t, 1H, *J* = 5 Hz), 5.09 (s, 2H), 3.71 (m, 4H), 3.42 (m, 2H), 3.22 (m, 6H). MS (ESI) 560.6 [M+H]⁺. Anal. (C₃₃H₃₃N₇O₂) C, H, N. HPLC analysis: retention time = 13.423 min; peak area, 98% (254 nm).

(5-(4-Hydroxyphenyl)-1-phenyl-1*H*-pyrazol-3-yl)(4-(pyrimidin-2-yl)piperazin-1-yl)methanone (8). White solid: yield 58%; mp 241 °C; ¹H NMR (200 MHz, DMSO-*d*₆): δ 9.86 (bs, 1H), 8.39 (d, 2H, *J* = 4.6 Hz), 7.42-7.35 (m, 5H), 7.04 (d, 2H, *J* = 8.6 Hz), 6.82 (s, 1H), 6.72 (d, 2H, *J* = 8.8 Hz), 6.68-6.66 (m, 1H), 4.14-4.08 (m, 2H), 3.84-3.71 (m, 6H). MS (ESI) 427.2 [M+H]⁺. Anal. (C₂₄H₂₂N₆O₂) C, H, N. HPLC analysis: retention time = 11.141 min; peak area, 95% (254 nm).

(5-(4-Hydroxyphenyl)-1-methyl-1*H*-pyrazol-3-yl)(4-(pyrimidin-2-yl)piperazin-1-yl)methanone (9). White solid: yield 30%; mp 209 °C; ¹H NMR (400 MHz, DMSO-*d*₆): δ 9,80 (bs, 1H), 8.39 (d, 2H, *J* = 4.8 Hz), 7.37(d, 2H, *J* = 8.4 Hz), 6.87 (d, 2H, *J* = 8,4 Hz), 6.74 (t, 1H, *J* = 4.8 Hz), 6.60 (s,

1H), 4.06-4.04 (m, 2H), 3.86 (s, 3H), 3.82-3.78 (m, 4H), 3.71-3.69 (m, 2H). MS (ESI) 365.1 [M+H]⁺.
Anal. (C₁₉H₂₀N₆O₂) C, H, N. HPLC analysis: retention time = 11.448 min; peak area, 96% (254 nm).

(5-(3-Hydroxyphenyl)-1-phenyl-1*H*-pyrazol-3-yl)(4-(pyrimidin-2-yl)piperazin-1-yl)methanone

(10). White solid: yield 25%; mp 122 °C; ¹H NMR (200 MHz, DMSO-*d*₆): δ 9.73 (bs, 1H), 8.39 (d, 2H, *J* = 4.0 Hz), 7.46-7.41 (m, 3H), 7.36-7.31 (m, 2H), 7.16 (t, 1H, *J* = 4.2 Hz), 6.88 (s, 1H), 6.77-6.64 (m, 4H), 4.10-4.06 (m, 2H), 3.84-3.71 (m, 6H). MS (ESI) 427.2 [M+H]⁺. Anal. (C₂₄H₂₂N₆O₂) C, H, N. HPLC analysis: retention time = 11.330 min; peak area, 96% (254 nm).

(5-(4-Hydroxyphenyl)-1-phenyl-1*H*-pyrazol-3-yl)(4-phenylpiperazin-1-yl)methanone (11).

White solid: yield 25%; mp 190 °C; ¹H NMR (200 MHz, DMSO-*d*₆): δ 9.78 (bs, 1H), 7.46-7.42 (m, 3H), 7.34-7.29 (m, 2H), 7.22-7.19 (m, 2H), 7.05 (d, 2H, *J* = 8.6 Hz), 6.98-6.94 (m, 2H), 6.83 (s, 1H), 6.80-6.78 (m, 1H), 6.70 (d, 2H, *J* = 8.6 Hz), 4.16-4.11 (m, 2H), 3.84-3.78 (m, 2H), 3.29-3.17 (m, 4H). MS (ESI) 425.2 [M+H]⁺. Anal. (C₂₆H₂₄N₄O₂) C, H, N. HPLC analysis: retention time = 12.327 min; peak area, 99% (254 nm).

(5-(4-Hydroxyphenyl)-1-phenyl-1*H*-pyrazol-3-yl)(4-methylpiperazin-1-yl)methanone (12).

White solid: yield 25%; mp 198 °C; ¹H NMR (200 MHz, DMSO-*d*₆): δ 9.82 (bs, 1H), 7.44-7.39 (m, 3H), 7.32-7.27 (m, 2H), 7.04 (d, 2H, *J* = 8.6 Hz), 6.77 (s, 1H), 6.71 (d, 2H, *J* = 8.6 Hz), 4.01-3.92 (m, 2H), 3.65-3.61 (m, 2H), 2.49 (s, 3H), 2.37-2.34 (m, 2H), 2.25-2.19 (s, 2H). MS (ESI) 363.2 [M+H]⁺. Anal. (C₂₁H₂₂N₄O₂) C, H, N. HPLC analysis: retention time = 12.972 min; peak area, 99% (254 nm).

(5-(4-Hydroxyphenyl)-1-phenyl-1*H*-pyrazol-3-yl)(morpholino)methanone (13).

White solid: yield 28%; mp 227 °C; ¹H NMR (200 MHz, DMSO-*d*₆): δ 9.85 (bs, 1H), 7.45-7.41 (m, 5H), 7.04 (d, 2H, *J* = 8.8 Hz), 6.80 (s, 1H), 6.71 (d, 2H, *J* = 8.6 Hz), 4.03-3.98 (m, 2H), 3.64 (s, 6H). MS (ESI) 350.1 [M+H]⁺. Anal. (C₂₀H₁₉N₃O₃) C, H, N. HPLC analysis: retention time = 9.682 min; peak area, 97% (254 nm).

(4-Benzylpiperazin-1-yl)(5-(4-hydroxyphenyl)-1-phenyl-1*H*-pyrazol-3-yl)methanone (14).

White solid: yield 40%; mp 169 °C; ¹H NMR (200 MHz, DMSO-*d*₆): δ 9.78 (bs, 1H), 7.43-7.38 (m, 3H), 7.33-7.26 (m, 7H), 7.03 (d, 2H, *J* = 8.4 Hz), 6.76 (s, 1H), 6.71 (d, 2H, *J* = 8.8 Hz), 3.98-3.93 (m, 2H), 3.67-3.62 (m,

2H), 3.51 (s, 2H), 2.50-2.41 (m, 4H). MS (ESI) 439.2 [M+H]⁺. Anal. (C₂₇H₂₆N₄O₂) C, H, N. HPLC analysis: retention time = 11.909 min; peak area, 98% (254 nm).

(4-Benzylpiperidin-1-yl)(5-(4-hydroxyphenyl)-1-phenyl-1H-pyrazol-3-yl)methanone (15).

White solid: yield 20%; mp 112 °C; ¹H NMR (400 MHz, DMSO-*d*₆): δ 9.78 (bs, 1H), 7.44-7.38 (m, 3H), 7.29-7.25 (m, 4H), 7.18-7.16 (m, 3H), 7.04 (d, 2H, *J* = 8.4 Hz), 6.73 (s, 1H), 6.72 (d, 2H, *J* = 8.4 Hz), 4.60 (d, 1H, *J* = 14 Hz), 4.48 (d, 1H, *J* = 12.4 Hz), 3.07 (t, 1H, *J* = 13.2 Hz), 2.69 (t, 1H, *J* = 13.2 Hz), 2.54-2.50 (m, 2H), 1.81-1.78 (m, 1H), 1.67-1.58 (m, 2H), 1.18-1.11 (m, 2H). MS (ESI) 438.2 [M+H]⁺. Anal. (C₂₈H₂₇N₃O₂) C, H, N. HPLC analysis: retention time = 13.132 min; peak area, 95% (254 nm).

***N*-(1-Benzylpiperidin-4-yl)-5-(4-hydroxyphenyl)-1-phenyl-1H-pyrazole-3-carboxamide (16).**

White solid: yield 20%; mp 200 °C; ¹H NMR (400 MHz, DMSO-*d*₆): δ 9.85 (bs, 1H), 8.03 (d, 1H, *J* = 8.0 Hz), 7.45-7.40 (m, 3H), 7.35-7.27 (m, 7H), 7.03 (d, 2H, *J* = 8.6 Hz), 6.85 (s, 1H), 6.70 (d, 2H, *J* = 8.4 Hz), 3.83-3.78 (m, 1H), 3.45 (s, 2H), 2.81 (d, 2H, *J* = 12.2 Hz), 2.10-1.98 (m, 2H), 1.69-1.63 (m, 4H). MS (ESI) 453.2 [M+H]⁺. Anal. (C₂₈H₂₈N₄O₂) C, H, N. HPLC analysis: retention time = 10.076 min; peak area, 98% (254 nm).

5-(4-Hydroxyphenyl)-1-phenyl-*N*-[2-(4-pyrimidin-2-yl)piperazin-1-yl]ethyl]-1H-pyrazole-3-carboxamide (17).

White solid: yield 20%; mp 217 °C; ¹H NMR (200 MHz, DMSO-*d*₆): δ 9.86 (bs, 1H), 8.34 (d, 2H, *J* = 4.6 Hz), 8.19 (t, 1H, *J* = 4.6 Hz), 7.45-7.40 (m, 3H), 7.35-7.30 (m, 2H), 7.04 (d, 2H, *J* = 8.4 Hz), 6.85 (s, 1H), 6.70 (d, 2H, *J* = 8.8 Hz), 6.63 (t, 1H, *J* = 5.0 Hz), 3.73-3.68 (m, 4H), 3.42-3.32 (m, 6H), 2.52-2.49 (m, 2H, *J* = 5.0 Hz). MS (ESI) 470.2 [M+H]⁺. Anal. (C₂₆H₂₇N₇O₂) C, H, N. HPLC analysis: retention time = 10.159 min; peak area, 98% (254 nm).

(4-Benzylpiperidin-1-yl)(5-(4-chlorophenyl)-1-phenyl-1H-pyrazol-3-yl)methanone (18).

White solid: yield 20%; mp 46 °C; ¹H NMR (200 MHz, DMSO-*d*₆): δ 7.46-7.21 (m, 5H), 7.33-7.19 (m, 9H), 6.92 (s, 1H), 4.61 (d, 1H, *J* = 14 Hz), 4.50 (d, 1H, *J* = 12.4 Hz), 3.07-2.72 (m, 2H), 2.54-2.49 (m, 2H), 1.85-1.80 (m, 1H), 1.65-1.59 (m, 2H), 1.17-1.11 (m, 2H). MS (ESI) 456.18 [M+H]⁺. Anal. (C₂₈H₂₆ClN₃O) C, H, N. HPLC analysis: retention time = 15.996 min; peak area, 96% (254 nm).

(4-Benzylpiperidin-1-yl)(1,5-diphenyl-1H-pyrazol-3-yl)methanone (19). White solid: yield 22%; mp 131 °C; ¹H NMR (400 MHz, DMSO-*d*₆): δ 7.45-7.16 (m, 15H), 6.88 (s, 1H), 4.42 (d, 1H, *J* = 14 Hz), 4.68 (d, 1H, *J* = 14 Hz), 3.22 (t, 1H, *J* = 13.4 Hz), 3.18 (t, 1H, *J* = 13.2 Hz), 1.98-1.94 (m, 1H), 2.58-2.56 (m, 2H), 1.75-1.65 (m, 2H), 1.55-1.22 (m, 2H). MS (ESI) 422.2 [M+H]⁺. Anal. (C₂₈H₂₇N₃O) C, H, N. HPLC analysis: retention time = 14.849 min; peak area, 98% (254 nm).

(4-Benzylpiperidin-1-yl)(5-(4-hydroxyphenyl)-1-(4-methoxyphenyl)-1H-pyrazol-3-yl)methanone (20). White solid: yield 25%; mp 128 °C; ¹H NMR (400 MHz, DMSO-*d*₆): δ 9.79 (bs, 1H), 7.27-7.16 (m, 6H), 7.04 (d, 2H, *J* = 8.8 Hz), 6.96 (d, 2H, *J* = 8.8 Hz), 6.72 (s, 1H), 6.71-6.70 (m, 3H), 4.61 (d, 1H, *J* = 12.8 Hz), 4.47 (d, 1H, *J* = 12.8 Hz), 3.77 (s, 3H), 3.05 (t, 1H, *J* = 12.4 Hz), 2.70 (t, 1H, *J* = 11.6 Hz), 2.54-2.50 (m, 2H), 1.85-1.79 (m, 1H), 1.67-1.57 (m, 2H), 1.16-1.08 (m, 2H). MS (ESI) 468.2 [M+H]⁺. Anal. (C₂₉H₂₉N₃O₃) C, H, N. HPLC analysis: retention time = 13.078 min; peak area, 95% (254 nm).

(4-Benzylpiperidin-1-yl)(1-(4-chlorophenyl)-5-(4-hydroxyphenyl)-1H-pyrazol-3-yl)methanone (21). White solid: yield 30%; mp 95 °C; ¹H NMR (400 MHz, DMSO-*d*₆): δ 9.83 (bs, 1H), 7.47 (d, 2H, *J* = 9.5.0 Hz), 7.24 (d, 2H, *J* = 9.6 Hz), 7.19-7.15 (m, 5H), 7.02 (d, 2H, *J* = 8.4 Hz), 6.72 (d, 2H, *J* = 8.4), 6.70 (s, 1H), 4.55-4.44 (m, 2H), 3.08 (t, 1H, *J* = 12.2 Hz), 2.75 (t, 1H, *J* = 11.8 Hz), 2.50-2.48 (m, 2H), 1.88-1.85 (m, 1H), 1.65-1.54 (m, 2H), 1.18-1.15 (m, 2H). MS (ESI) 471.1 [M+H]⁺. Anal. (C₂₈H₂₆ClN₃O₂) C, H, N. HPLC analysis: retention time = 13.757 min; peak area, 95% (254 nm).

(4-Benzylpiperidin-1-yl)(5-(4-hydroxyphenyl)-1-(*p*-tolyl)-1H-pyrazol-3-yl)methanone (22). White solid: yield 45%; mp 126 °C; ¹H NMR (200 MHz, DMSO-*d*₆): δ 9.80 (bs, 1H), 7.24-7.17 (m, 9H), 7.05 (d, 2H, *J* = 8.4 Hz), 6.73 (d, 2H, *J* = 8.4 Hz), 6.69 (s, 1H), 4.56-4.48 (m, 2H), 3.08 (t, 1H, *J* = 11.8 Hz), 2.80 (t, 1H, *J* = 12.0 Hz), 2.50-2.38 (m, 2H), 2.32 (s, 3H), 1.89-1.85 (m, 3H), 1.17-1.15 (m, 2H). MS (ESI) 451.2 [M+H]⁺. Anal. (C₂₉H₂₉N₃O₂) C, H, N. HPLC analysis: retention time = 13.518 min; peak area, 98% (254 nm).

(1-Benzyl-5-(4-hydroxyphenyl)-1H-pyrazol-3-yl)(4-benzylpiperidin-1-yl)methanone (23). White solid: yield 48%; mp 84 °C; ¹H NMR (200 MHz, DMSO-*d*₆): δ 9.90 (bs, 1H), 7.29-7.15 (m,

10H), 7.02-6.79 (m, 4H), 6.55 (s, 1H), 5.34 (s, 2H), 4.62-4.35 (m, 2H), 3.13-2.93 (m, 1H), 2.74-2.55 (m, 1H), 2.54 (m, 2H), 1.92-1.73 (m, 1H), 1.72-1.48 (m, 2H), 1.25-1.02 (m, 2H). MS (ESI) 452.2 [M+H]⁺. Anal. (C₂₉H₂₉N₃O₂) C, H, N. HPLC analysis: retention time = 13.198 min; peak area, 100% (254 nm).

(4-Benzylpiperidin-1-yl)(5-(4-hydroxyphenyl)-1-phenethyl-1H-pyrazol-3-yl)methanone (24).

White solid: yield 58%; mp 70 °C; ¹H NMR (200 MHz, DMSO-*d*₆): δ 9.92 (bs, 1H), 7.29-7.16 (m, 8H), 7.05 (d, 2H, *J* = 8.4 Hz), 6.98-6.94 (m, 2H), 6.80 (d, 2H, *J* = 8.4 Hz), 6.39 (s, 1H), 4.47-4.40 (m, 2H), 4.25 (t, 2H, *J* = 7.0 Hz), 2.99 (t, 2H, *J* = 7.0 Hz), 2.74-2.54 (m, 4H), 1.99-1.96 (m, 1H), 1.72-1.52 (m, 2H), 1.21-1.05 (m, 2H). MS (ESI) 466.2 [M+H]⁺. Anal. (C₃₀H₃₁N₃O₂) C, H, N. HPLC analysis: retention time = 13.374 min; peak area, 98% (254 nm).

(4-Benzylpiperidin-1-yl)(5-(4-hydroxyphenyl)-1-(3-phenylpropyl)-1H-pyrazol-3-yl)methanone (25).

White solid: yield 55%; mp 67 °C; ¹H NMR (200 MHz, DMSO-*d*₆): δ 9.94 (bs, 1H), 7.27-7.06 (m, 12H), 6.85 (d, 2H, *J* = 8.4 Hz), 6.47 (s, 1H), 4.70-4.59 (m, 2H), 4.07 (t, 2H, *J* = 6.8), 3.16-2.98 (m, 1H), 2.78-2.68 (m, 1H), 2.55-2.46 (m, 4H), 2.11-1.95 (m, 2H), 1.91-1.78 (m, 1H), 1.77-1.51 (m, 2H), 1.23-1.18 (m, 2H). MS (ESI) 480.2 [M+H]⁺. Anal. (C₃₁H₃₃N₃O₂) C, H, N. HPLC analysis: retention time = 13.835 min; peak area, 99% (254 nm).

(4-Benzylpiperidin-1-yl)(5-(4-hydroxyphenyl)-1-(3-methylbenzyl)-1H-pyrazol-3-yl)methanone (26).

White solid: yield 50%; mp 70 °C; ¹H NMR (200 MHz, DMSO-*d*₆): δ 9.81 (bs, 1H), 7.24-7.17 (m, 9H), 6.84-6.80 (m, 4H), 6.54 (s, 1H), 5.29 (s, 2H), 4.50-4.42 (m, 2H), 3.20-2.98 (m, 1H), 2.78-2.56 (m, 1H), 2.52-2.48 (m, 2H), 2.21 (s, 3H), 1.98-1.42 (m, 3H), 1.21-1.05 (m, 2H). MS (ESI) 466.2 [M+H]⁺. Anal. (C₃₀H₃₁N₃O₂) C, H, N. HPLC analysis: retention time = 13.534 min; peak area, 99% (254 nm).

(4-Benzylpiperidin-1-yl)(5-(4-hydroxyphenyl)-1-(4-methylbenzyl)-1H-pyrazol-3-yl)methanone (27).

White solid: yield 68%; mp 160 °C; ¹H NMR (200 MHz, DMSO-*d*₆): δ 9.91 (bs, 1H), 7.28-7.07 (m, 9H), 6.89-6.80 (m, 4H), 6.53 (s, 1H), 5.29 (s, 2H), 4.58-4.41 (m, 2H), 3.18-2.98 (m, 1H), 2.79-2.58 (m, 1H), 2.54-

2.49 (m, 2H), 2.23 (s, 3H), 1.98-1.52 (m, 3H), 1.21-1.04 (m, 2H). MS (ESI) 466.2 [M+H]⁺. Anal. (C₃₀H₃₁N₃O₂) C, H, N. HPLC analysis: retention time = 13.595 min; peak area, 98% (254 nm).

(4-Benzylpiperidin-1-yl)(1-(3,5-dimethylbenzyl)-5-(4-hydroxyphenyl)-1H-pyrazol-3-yl)methanone (28). White solid: yield 78%; mp 74 °C; ¹H NMR (200 MHz, DMSO-*d*₆): δ 9.91 (bs, 1H), 7.27-7.15 (m, 7H), 6.87-6.81 (m, 3H), 6.59-6.53 (m, 3H), 5.24 (s, 2H), 4.57-4.41 (m, 2H), 3.20-2.99 (m, 1H), 2.79-2.60 (m, 1H), 2.55-2.48 (m, 2H), 2.17 (s, 6H), 1.93-1.50 (m, 3H), 1.22-1.05 (m, 2H). MS (ESI) 480.2 [M+H]⁺. Anal. (C₃₁H₃₃N₃O₂) C, H, N. HPLC analysis: retention time = 14.028 min; peak area, 99% (254 nm).

(4-Benzylpiperidin-1-yl)(5-(4-hydroxyphenyl)-1-(naphthalen-1-ylmethyl)-1H-pyrazol-3-yl)methanone (29). White solid: yield 55%; mp 122 °C; ¹H NMR (200 MHz, DMSO-*d*₆): δ 9.98 (bs, 1H), 7.99-7.85 (m, 3H), 7.54-7.13 (m, 10H), 6.81-6.73 (m, 3H), 6.60 (s, 1H), 5.83 (s, 2H), 4.47-4.42 (m, 2H), 3.21-3.11 (m, 1H), 2.71-2.69 (m, 1H), 2.54-2.51 (m, 2H), 1.93-1.50 (m, 3H), 1.22-1.04 (m, 2H). MS (ESI) 502.2 [M+H]⁺. Anal. (C₃₃H₃₁N₃O₂) C, H, N. HPLC analysis: retention time = 13.888 min; peak area, 98% (254 nm).

General procedure for the synthesis of ethyl 1,5-diphenylpyrazole-3-carboxylates (30a-p). A mixture of 2,4-dioxobutanoate (6.3 mmol) and appropriate hydrazine (7.5 mmol) in absolute EtOH (30 mL) was stirred at 80 °C for 5 h. The solvent was removed under reduced pressure after the reaction had reached completion. Then the residue was purified by column chromatography on silica gel via elution with an appropriate mixture of ethyl acetate and petroleum ether to give the desired product.

Ethyl 5-[4-(benzyloxy)phenyl]-1-phenyl-1H-pyrazole-3-carboxylate (30a). White solid: yield 70%; mp 124-125 °C; ¹H NMR (200 MHz, DMSO-*d*₆) δ 7.33-7.45 (m, 10H), 7.18 (d, 2H, *J* = 8.8 Hz), 7.03 (d, 2H, *J* = 8.4 Hz), 6.96 (s, 1H), 5.09 (s, 2H), 4.32 (q, *J* = 7.0 Hz, 2H), 1.31 (t, 3H, *J* = 7.0 Hz). MS (ESI) 392.2 [M+H]⁺.

Ethyl 5-(4-hydroxyphenyl)-1-(4-methoxyphenyl)-1H-pyrazole-3-carboxylate (30d). White solid: yield 67%; mp 177-178 °C; ¹H NMR (200 MHz, DMSO-*d*₆) δ 9.75 (bs, 1H), 7.25 (d, 2H, *J* = 9 Hz),

7.04 (d, 2H, $J = 8.6$ Hz), 7.00 (d, 2H, $J = 9.2$ Hz), 6.88 (s, 1H), 6.71 (d, 2H, $J = 8.6$ Hz), 4.28 (q, 2H, $J = 7$ Hz), 3.78 (s, 3H), 1.30 (t, 3H, $J = 7$ Hz). MS (ESI) 339.1 [M+H]⁺.

Ethyl 5-(4-hydroxyphenyl)-1-(*p*-tolyl)-1*H*-pyrazole-3-carboxylate (30f). White solid; yield 62%; mp 199-200 °C; ¹H NMR (200 MHz, DMSO-*d*₆) δ 9.82 (bs, 1H), 7.22 (d, 2H, $J = 8.8$ Hz), 7.02 (d, 2H, $J = 8.6$ Hz), 6.95 (d, 2H, $J = 8.8$ Hz), 6.88 (s, 1H), 6.67 (d, 2H, $J = 8.6$ Hz), 4.30 (q, 2H, $J = 7$ Hz), 2.28 (s, 3H), 1.30 (t, 3H, $J = 7$ Hz). MS (ESI) 322.1 [M+H]⁺.

*Ethyl 1-benzyl-5-(4-hydroxyphenyl)-1*H*-pyrazole-3-carboxylate (30g).* White solid; yield 50%; mp 79-81 °C; ¹H NMR (200 MHz, DMSO-*d*₆): δ 9.87 (bs, 1H), 7.27-7.22 (m, 5H), 6.99-6.95 (m, 2H), 6.85-6.80 (m, 3H), 5.42 (s, 2H), 4.28 (q, 2H, $J = 7.2$ Hz), 1.29 (t, 3H, $J = 7.0$ Hz). MS (ESI) 323.1 [M+H]⁺.

Ethyl 5-(4-hydroxyphenyl)-1-(2-phenylethyl)-1*H*-pyrazole-3-carboxylate (30h). Light yellow solid; yield 40%; mp 190-192 °C; ¹H NMR (200 MHz, DMSO-*d*₆): δ 9.98 (bs, 1H), 7.23-7.20 (m, 2H), 7.07 (m, 5H), 6.82-6.77 (m, 2H), 6.66 (s, 1H), 4.34-4.27 (m, 4H), 3.04 (t, 2H, $J = 8.3$ Hz), 1.30 (t, 2H, $J = 7.0$ Hz). MS (ESI) 337.1 [M+H]⁺.

Ethyl 5-(4-hydroxyphenyl)-1-(3-phenylpropyl)-1*H*-pyrazole-3-carboxylate (30i). Light yellow solid; yield 48%; mp 126-128 °C. ¹H NMR (200 MHz, DMSO-*d*₆): δ 9.95 (bs, 1H), 7.25-7.05 (m, 7H), 6.83-6.79 (m, 2H), 6.69 (s, 1H), 4.26 (q, 2H, $J = 7.0$ Hz), 4.11 (t, 2H, $J = 7.3$ Hz), 2.58 (t, 2H, $J = 8.3$ Hz), 2.10-1.92 (m, 2H), 1.27 (t, 3H, $J = 7.0$ Hz). MS (ESI) 351.2 [M+H]⁺.

Ethyl 5-(4-hydroxyphenyl)-1-(3-methylbenzyl)-1*H*-pyrazole-3-carboxylate (30j). White solid; yield 81%; mp 173-175 °C; ¹H NMR (200 MHz, DMSO-*d*₆): δ 9.96 (bs, 1H), 7.26-7.00 (m, 4H), 6.85-6.69 (m, 5H), 5.37 (s, 2H), 4.28 (q, 2H, $J = 7.2$), 2.23 (s, 1H), 1.29 (t, 3H, $J = 7.2$ Hz). MS (ESI) 337.1 [M+H]⁺.

Ethyl 5-(4-hydroxyphenyl)-1-(4-methylbenzyl)-1*H*-pyrazole-3-carboxylate (30k). White solid; yield 80%; mp 147-148 °C; ¹H NMR (200 MHz, DMSO-*d*₆): δ 9.97 (s, 1H), 7.24 (d, 2H, $J = 8.4$), 7.52 (d, 2H, $J = 7.8$ Hz), 6.84-6.79 (m, 5H), 5.36 (s, 2H), 4.27 (q, 2H, $J = 7.2$), 2.24 (s, 3H), 1.28 (t, 3H, $J = 7.2$ Hz). MS (ESI) 337.1 [M+H]⁺.

Ethyl 1-(3,5-dimethylbenzyl)-5-(4-hydroxyphenyl)-1H-pyrazole-3-carboxylate (30l). White solid: yield 64%; mp 162-163 °C; ¹H NMR (200 MHz, DMSO-*d*₆): δ 9.98 (bs, 1H), 7.26-7.21 (m, 2H), 6.88-6.79 (m, 4H), 6.56 (s, 2H), 5.31 (s, 2H), 4.28 (q, 2H, *J* = 7.0 Hz), 2.18 (s, 6H), 1.28 (t, 3H, *J* = 7.0 Hz). MS (ESI) 351.2 [M+H]⁺.

Ethyl 5-(4-hydroxyphenyl)-1-(1-naphthylmethyl)-1H-pyrazole-3-carboxylate (30m). White solid: yield 54%; mp 215-216 °C; ¹H NMR (200 MHz, DMSO-*d*₆): δ 9.95 (bs, 1H), 7.97-7.84 (m, 3H), 7.57-7.24 (m, 5H), 6.89 (s, 1H), 6.79-6.69 (m, 3H), 5.91 (s, 2H), 4.28 (q, 2H, *J* = 7.0 Hz), 1.28 (t, 3H, *J* = 7.0 Hz). MS (ESI) 373.2 [M+H]⁺.

Ethyl 1,5-diphenyl-1H-pyrazole-3-carboxylate (30o). White solid: yield 64%; mp 82-84 °C; ¹H NMR (200 MHz, DMSO-*d*₆): δ 7.46-7.28 (m, 10H), 7.13 (s, 1H), 4.34 (q, 2H, *J* = 7.4 Hz), 1.32 (t, 3H, *J* = 7.0 Hz). MS (ESI) 293.1 [M+H]⁺.

Ethyl 5-(4-chlorophenyl)-1-phenyl-1H-pyrazole-3-carboxylate (30p). Light yellow solid; yield 55%; mp 95-97 °C; ¹H NMR (200 MHz, DMSO-*d*₆): δ 7.47-7.25 (m, 9H), 7.17 (s, 1H), 4.34 (q, 2H, *J* = 8.0 Hz), 1.32 (t, 3H, *J* = 7.2 Hz). MS (ESI) 327.1 [M+H]⁺.

General procedure for the synthesis of 1,5-diphenylpyrazole-3-carboxylic acids (31a-p). To a solution of the esters **30a-p** (2.0 mmol) in ethanol (30 mL) was added aqueous sodium hydroxide (10%, 8 mL). The resulting mixture was stirred at 60 °C for 4 h. The solvent was evaporated under reduced pressure, and the residue was acidified with 10% hydrochloric acid at 0 °C. The precipitate thus formed was collected by filtration, washed with water, and dried under vacuum to give the desired carboxylic acid.

5-[4-(Benzyloxy)phenyl]-1-phenyl-1H-pyrazole-3-carboxylic acid (31a). White solid: yield 80%; mp 168-169 °C; ¹H NMR (200 MHz, DMSO-*d*₆) δ 12.3 (bs, 1H), 7.47-7.34 (m, 10H), 7.17 (d, 2H, *J* = 8.8 Hz), 7.01-6.97 (m, 3H), 5.09 (s, 2H). MS (ESI) 371.1 [M+H]⁺.

5-(4-Hydroxyphenyl)-1-(4-methoxyphenyl)-1H-pyrazole-3-carboxylic acid (31d). White solid: yield 84%; mp 197-198 °C; ¹H NMR (200 MHz, DMSO-*d*₆) δ 12.80 (bs, 1H), 9.85 (bs, 1H), 7.23 (d,

2H, $J = 9$ Hz), 7.4 (d, 2H, $J = 8.6$ Hz), 7.0 (d, $J = 9.2$ Hz, 2H), 6.88 (s, 1H), 6.71 (d, 2H, $J = 8.6$ Hz), 3.78 (s, 3H). MS (ESI) 311.1 [M+H]⁺.

5-(4-Hydroxyphenyl)-1-(p-tolyl)-1H-pyrazole-3-carboxylic acid (31f). White solid: yield 75%; mp 234 °C; ¹H NMR (200 MHz, DMSO-*d*₆) δ 12.80 (bs, 1H), 9.85 (bs, 1H), 7.23 (d, 2H, $J = 8.8$ Hz), 7.16 (d, 2H, $J = 8.4$ Hz), 7.05 (d, 2H, $J = 8.8$ Hz), 6.89 (s, 1H), 6.71 (d, 2H, $J = 8.8$ Hz), 2.33 (s, 3H). MS (ESI) 294.1 [M+H]⁺.

1-Benzyl-5-(4-hydroxyphenyl)-1H-pyrazole-3-carboxylic acid (31g). White solid: yield 80%; mp 244-246 °C; ¹H NMR (200 MHz, DMSO-*d*₆): δ 12.89 (bs, 1H), 9.87 (bs, 1H), 7.31-7.21 (m, 5H), 7.01-6.96- (m, 2H), 6.84-6.80 (m, 2H), 6.73 (s, 1H), 5.39 (s, 2H). MS (ESI) 295.1 [M+H]⁺.

5-(4-Hydroxyphenyl)-1-(2-phenylethyl)-1H-pyrazole-3-carboxylic acid (31h). White solid: yield 87%; mp 198-199 °C; ¹H NMR (200 MHz, DMSO-*d*₆): δ 13.11 (bs, 1H), 9.98 (bs, 1H), 7.23-7.20 (m, 2H), 7.06-6.97 (m, 5H), 6.82-6.77 (m, 2H), 6.60 (s, 1H), 4.28 (t, 2H, $J = 6.9$ Hz), 3.04 (t, 2H, $J = 7.8$ Hz). MS (ESI) 309.1 [M+H]⁺.

5-(4-Hydroxyphenyl)-1-(3-phenylpropyl)-1H-pyrazole-3-carboxylic acid (31i). White solid: yield 75%; mp 196-198 °C; ¹H NMR (200 MHz, DMSO-*d*₆): δ 13.10 (bs, 1H), 9.95 (bs, 1H), 7.33-7.16 (m, 7H), 6.97-6.92 (m, 2H), 6.71 (s, 1H), 4.19 (t, 2H, $J = 7.2$), 2.58 (t, 2H, $J = 8.3$ Hz), 1.99 (m, 2H). MS (ESI) 323.1 [M+H]⁺.

5-(4-Hydroxyphenyl)-1-(3-methylbenzyl)-1H-pyrazole-3-carboxylic acid (31j). White solid: yield 80%; mp 207-208 °C; ¹H NMR (200 MHz, DMSO-*d*₆): δ 12.85 (bs, 1H), 9.20 (bs, 1H), 7.25-7.02 (m, 4H), 6.85-6.73 (m, 5H), 5.34 (s, 2H), 2.23 (s, 3H). MS (ESI) 309.1 [M+H]⁺.

5-(4-Hydroxyphenyl)-1-(4-methylbenzyl)-1H-pyrazole-3-carboxylic acid (31k). White solid: yield 88%; mp 242-243 °C; ¹H NMR (200 MHz, DMSO-*d*₆): δ 13.20 (bs, 1H), 10.00 (bs, 1H), 7.25-7.08 (m, 4H), 6.90-6.80 (m, 4H), 6.73 (s, 1H), 5.34 (s, 2H), 2.25 (s, 3H). MS (ESI) 309.1 [M+H]⁺.

1-(3,5-Dimethylbenzyl)-5-(4-hydroxyphenyl)-1H-pyrazole-3-carboxylic acid (31l). White solid: yield 88%; mp 240-242 °C; ¹H NMR (200 MHz, DMSO-*d*₆): δ 12.88 (bs, 1H), 9.81 (bs, 1H), 7.25-7.20 (m, 4H), 6.88-6.81 (m, 3H), 6.71 (s, 1H), 5.29 (s, 2H), 2.19 (s, 6H). MS (ESI) 323.1 [M+H]⁺.

5-(4-Hydroxyphenyl)-1-((naphthalen-1-yl)methyl)-1*H*-pyrazole-3-carboxylic acid (31m). White solid: yield 90%; mp 251-252 °C; ¹H NMR (200 MHz, DMSO-*d*₆): δ 12.85 (bs, 1H), 9.82 (bs, 1H), 7.99-7.34 (m, 3H), 7.57-7.37 (m, 3H), 7.27-7.23 (m, 2H), 6.82-6.69 (m, 4H), 5.88 (s, 2H). MS (ESI) 345.1 [M+H]⁺.

1,5-Diphenyl-1*H*-pyrazole-3-carboxylic acid (31o). White solid: yield 85%; mp 182-183 °C; ¹H NMR (200 MHz, DMSO-*d*₆): δ 12.99 (bs, 1H), 7.40-7.17 (m, 10H), 6.74 (s, 1H). MS (ESI) 265.1 [M+H]⁺.

5-(4-Chlorophenyl)-1-phenyl-1*H*-pyrazole-3-carboxylic acid (31p). White solid: yield 75%; mp >300 °C; ¹H NMR (200 MHz, DMSO-*d*₆): δ 12.95 (bs, 1H), 7.41-7.17 (m, 9H), 6.75 (s, 1H). MS (ESI) 299.1 [M+H]⁺.

ASSOCIATED CONTENT

Supporting Information

The Supporting Information is available free of charge on the ACS Publications website at DOI: XXXX.

General binding hypothesis for the design of diphenylpyrazole MAGL inhibitors, LC-MS/MS quantification of endocannabinoids and other metabolites, HPLC chromatograms of the final compounds.

AUTHOR INFORMATION

Corresponding Author

*Phone: +39 050 2219595. Fax: +39 050 2210680. E-mail: tiziano.tuccinardi@unipi.it.

ORCID

Tiziano Tuccinardi: 0000-0002-6205-4069

Notes

The authors declare no competing financial interest.

ABBREVIATIONS USED

MAGL, monoacylglycerol lipase; GPCRs, G protein-coupled receptors; FABPs, fatty acid binding proteins; FAAH, fatty acid amide hydrolase; NAAA, *N*-acylethanolamine hydrolyzing acid amidase; DAGL, diacylglycerol lipases; 2-AG, 2-arachidonoylglycerol; AEA, anandamide; VR1, vanilloid receptor 1; TRPV1, transient potential vanilloid type 1; NAM, *N*-Arachidonoyl maleimide; ABHD6, α/β -hydrolase domain-containing 6; ABHD12, α/β -hydrolase domain-containing 12; HG-SOC, high-grade serous ovarian cancer; PAINS, pan assay interference compounds; BSA, bovine serum albumin; CG, conjugate gradient; 4-NPA, 4-nitrophenylacetate; AA, arachidonic acid; PGE2, prostaglandin-E2; PGD2, prostaglandin-D2; DRG, dorsal root ganglia.

ACKNOWLEDGMENTS

We are grateful to the University of Pisa (Progetti di Ricerca di Ateneo, PRA_2017_51) for funding.

REFERENCES

1. Pertwee, R. G. Emerging strategies for exploiting cannabinoid receptor agonists as medicines. *Br. J. Pharmacol.* **2009**, *156*, 397-411.
2. Pacher, P.; Batkai, S.; Kunos, G. The endocannabinoid system as an emerging target of pharmacotherapy. *Pharmacol. Rev* **2006**, *58*, 389-462.
3. Ahn, K.; McKinney, M. K.; Cravatt, B. F. Enzymatic pathways that regulate endocannabinoid signaling in the nervous system. *Chem. Rev.* **2008**, *108*, 1687-1707.
4. Di Marzo, V. Targeting the endocannabinoid system: to enhance or reduce? *Nat. Rev. Drug discovery* **2008**, *7*, 438-455.
5. Alger, B. E.; Kim, J. Supply and demand for endocannabinoids. *Trends Neurosci.* **2011**, *34*, 304-315.
6. Maccarrone, M.; Guzman, M.; Mackie, K.; Doherty, P.; Harkany, T. Programming of neural cells by (endo)cannabinoids: from physiological rules to emerging therapies. *Nat. Rev. Neurosci.* **2014**, *15*, 786-801.

7. Chicca, A.; Marazzi, J.; Nicolussi, S.; Gertsch, J. Evidence for bidirectional endocannabinoid transport across cell membranes. *J. Biol. Chem.* **2012**, *287*, 34660-34682.
8. Chicca, A.; Nicolussi, S.; Bartholomaeus, R.; Blunder, M.; Aparisi Rey, A.; Petrucci, V.; Reynoso-Moreno, I. D. C.; Viveros-Paredes, J. M.; Dalghi Gens, M.; Lutz, B.; Schioth, H. B.; Soeberdt, M.; Abels, C.; Charles, R. P.; Altmann, K. H.; Gertsch, J. Chemical probes to potently and selectively inhibit endocannabinoid cellular reuptake. *P. Natl. Acad. Sci. USA* **2017**, *114*, E5006-E5015.
9. Kaczocha, M.; Glaser, S. T.; Deutsch, D. G. Identification of intracellular carriers for the endocannabinoid anandamide. *P. Natl. Acad. Sci. USA* **2009**, *106*, 6375-6380.
10. Oddi, S.; Fezza, F.; Pasquariello, N.; D'Agostino, A.; Catanzaro, G.; De Simone, C.; Rapino, C.; Finazzi-Agro, A.; Maccarrone, M. Molecular identification of albumin and Hsp70 as cytosolic anandamide-binding proteins. *Chem. Biol.* **2009**, *16*, 624-632.
11. Bisogno, T.; De Petrocellis, L.; Di Marzo, V. Fatty acid amide hydrolase, an enzyme with many bioactive substrates. Possible therapeutic implications. *Curr. Pharm. Design* **2002**, *8*, 533-547.
12. Sugiura, T.; Kobayashi, Y.; Oka, S.; Waku, K. Biosynthesis and degradation of anandamide and 2-arachidonoylglycerol and their possible physiological significance. *Prostag. Leukotr. Ess.* **2002**, *66*, 173-192.
13. Bequet, F.; Uzabiaga, F.; Desbazeille, M.; Ludwiczak, P.; Maftouh, M.; Picard, C.; Scatton, B.; Le Fur, G. CB1 receptor-mediated control of the release of endocannabinoids (as assessed by microdialysis coupled with LC/MS) in the rat hypothalamus. *Eur. J. Neurosci.* **2007**, *26*, 3458-3464.
14. Caille, S.; Alvarez-Jaimes, L.; Polis, I.; Stouffer, D. G.; Parsons, L. H. Specific alterations of extracellular endocannabinoid levels in the nucleus accumbens by ethanol, heroin, and cocaine self-administration. *J. Neurosci.* **2007**, *27*, 3695-3702.
15. Ross, R. A. Anandamide and vanilloid TRPV1 receptors. *Br. J. Pharmacol.* **2003**, *140*, 790-801.

16. Lichtman, A. H.; Leung, D.; Shelton, C. C.; Saghatelian, A.; Hardouin, C.; Boger, D. L.; Cravatt, B. F. Reversible inhibitors of fatty acid amide hydrolase that promote analgesia: evidence for an unprecedented combination of potency and selectivity. *J. Pharmacol. Exp. Ther.* **2004**, *311*, 441-448.
17. Blankman, J. L.; Cravatt, B. F. Chemical probes of endocannabinoid metabolism. *Pharmacol. Rev.* **2013**, *65*, 849-871.
18. Hohmann, A. G.; Suplita, R. L.; Bolton, N. M.; Neely, M. H.; Fegley, D.; Mangieri, R.; Krey, J. F.; Walker, J. M.; Holmes, P. V.; Crystal, J. D.; Duranti, A.; Tontini, A.; Mor, M.; Tarzia, G.; Piomelli, D. An endocannabinoid mechanism for stress-induced analgesia. *Nature* **2005**, *435*, 1108-1112.
19. Vandevorde, S.; Jonsson, K. O.; Labar, G.; Persson, E.; Lambert, D. M.; Fowler, C. J. Lack of selectivity of URB602 for 2-oleoylglycerol compared to anandamide hydrolysis in vitro. *Br. J. Pharmacol.* **2007**, *150*, 186-191.
20. Muccioli, G. G.; Xu, C.; Odah, E.; Cudaback, E.; Cisneros, J. A.; Lambert, D. M.; Lopez Rodriguez, M. L.; Bajjalieh, S.; Stella, N. Identification of a novel endocannabinoid-hydrolyzing enzyme expressed by microglial cells. *J. Neurosci.* **2007**, *27*, 2883-2889.
21. Comelli, F.; Giagnoni, G.; Bettoni, I.; Colleoni, M.; Costa, B. The inhibition of monoacylglycerol lipase by URB602 showed an anti-inflammatory and anti-nociceptive effect in a murine model of acute inflammation. *Br. J. Pharmacol.* **2007**, *152*, 787-794.
22. Desroches, J.; Charron, S.; Bouchard, J. F.; Beaulieu, P. Endocannabinoids decrease neuropathic pain-related behavior in mice through the activation of one or both peripheral CB(1) and CB(2) receptors. *Neuropharmacology* **2014**, *77*, 441-452.
23. Saario, S. M.; Salo, O. M.; Nevalainen, T.; Poso, A.; Laitinen, J. T.; Jarvinen, T.; Niemi, R. Characterization of the sulfhydryl-sensitive site in the enzyme responsible for hydrolysis of 2-arachidonoyl-glycerol in rat cerebellar membranes. *Chem. Biol.* **2005**, *12*, 649-656.

24. Bisogno, T.; Ortar, G.; Petrosino, S.; Morera, E.; Palazzo, E.; Nalli, M.; Maione, S.; Di Marzo, V. Development of a potent inhibitor of 2-arachidonoylglycerol hydrolysis with antinociceptive activity in vivo. *Biochim. Biophys. Acta* **2009**, *1791*, 53-60.
25. Minkkila, A.; Saario, S.; Nevalainen, T. Discovery and development of endocannabinoid-hydrolyzing enzyme inhibitors. *Curr. Top. Med. Chem.* **2010**, *10*, 828-858.
26. Petrosino, S.; Di Marzo, V. FAAH and MAGL inhibitors: therapeutic opportunities from regulating endocannabinoid levels. *Curr. Opin. Investig. Drugs* **2010**, *11*, 51-62.
27. Nomura, D. K.; Morrison, B. E.; Blankman, J. L.; Long, J. Z.; Kinsey, S. G.; Marcondes, M. C.; Ward, A. M.; Hahn, Y. K.; Lichtman, A. H.; Conti, B.; Cravatt, B. F. Endocannabinoid hydrolysis generates brain prostaglandins that promote neuroinflammation. *Science* **2011**, *334*, 809-813.
28. Nomura, D. K.; Long, J. Z.; Niessen, S.; Hoover, H. S.; Ng, S. W.; Cravatt, B. F. Monoacylglycerol lipase regulates a fatty acid network that promotes cancer pathogenesis. *Cell* **2010**, *140*, 49-61.
29. Long, J. Z.; Li, W.; Booker, L.; Burston, J. J.; Kinsey, S. G.; Schlosburg, J. E.; Pavon, F. J.; Serrano, A. M.; Selley, D. E.; Parsons, L. H.; Lichtman, A. H.; Cravatt, B. F. Selective blockade of 2-arachidonoylglycerol hydrolysis produces cannabinoid behavioral effects. *Nat. Chem. Biol.* **2009**, *5*, 37-44.
30. Schlosburg, J. E.; Blankman, J. L.; Long, J. Z.; Nomura, D. K.; Pan, B.; Kinsey, S. G.; Nguyen, P. T.; Ramesh, D.; Booker, L.; Burston, J. J.; Thomas, E. A.; Selley, D. E.; Sim-Selley, L. J.; Liu, Q. S.; Lichtman, A. H.; Cravatt, B. F. Chronic monoacylglycerol lipase blockade causes functional antagonism of the endocannabinoid system. *Nat. Neurosci.* **2010**, *13*, 1113-1119.
31. Cisneros, J. A.; Bjorklund, E.; Gonzalez-Gil, I.; Hu, Y.; Canales, A.; Medrano, F. J.; Romero, A.; Ortega-Gutierrez, S.; Fowler, C. J.; Lopez-Rodriguez, M. L. Structure-activity relationship of a new series of reversible dual monoacylglycerol lipase/fatty acid amide hydrolase inhibitors. *J. Med. Chem.* **2012**, *55*, 824-836.

32. Hernandez-Torres, G.; Cipriano, M.; Heden, E.; Bjorklund, E.; Canales, A.; Zian, D.; Feliu, A.; Mecha, M.; Guaza, C.; Fowler, C. J.; Ortega-Gutierrez, S.; Lopez-Rodriguez, M. L. A reversible and selective inhibitor of monoacylglycerol lipase ameliorates multiple sclerosis. *Angew. Chem. Int. Ed. Engl.* **2014**, *53*, 13765-13770.
33. Patel, J. Z.; Ahenkorah, S.; Vaara, M.; Staszewski, M.; Adams, Y.; Laitinen, T.; Navia-Paldanius, D.; Parkkari, T.; Savinainen, J. R.; Walczynski, K.; Laitinen, J. T.; Nevalainen, T. J. Loratadine analogues as MAGL inhibitors. *Bioorg. Med. Chem. Lett.* **2015**, *25*, 1436-1442.
34. Granchi, C.; Rizzolio, F.; Palazzolo, S.; Carmignani, S.; Macchia, M.; Saccomanni, G.; Manera, C.; Martinelli, A.; Minutolo, F.; Tuccinardi, T. Structural optimization of 4-chlorobenzoylpiperidine derivatives for the development of potent, reversible, and selective monoacylglycerol lipase (MAGL) inhibitors. *J. Med. Chem.* **2016**, *59*, 10299-10314.
35. Schalk-Hihi, C.; Schubert, C.; Alexander, R.; Bayoumy, S.; Clemente, J. C.; Deckman, I.; DesJarlais, R. L.; Dzordzorme, K. C.; Flores, C. M.; Grasberger, B.; Kranz, J. K.; Lewandowski, F.; Liu, L.; Ma, H.; Maguire, D.; Macielag, M. J.; McDonnell, M. E.; Mezzasalma Haarlander, T.; Miller, R.; Milligan, C.; Reynolds, C.; Kuo, L. C. Crystal structure of a soluble form of human monoglyceride lipase in complex with an inhibitor at 1.35 Å resolution. *Protein Sci.* **2011**, *20*, 670-683.
36. Tuccinardi, T.; Granchi, C.; Rizzolio, F.; Caligiuri, I.; Battistello, V.; Toffoli, G.; Minutolo, F.; Macchia, M.; Martinelli, A. Identification and characterization of a new reversible MAGL inhibitor. *Bioorg. Med. Chem.* **2014**, *22*, 3285-3291.
37. Muccioli, G. G.; Labar, G.; Lambert, D. M. CAY10499, a novel monoglyceride lipase inhibitor evidenced by an expeditious MGL assay. *Chembiochem* **2008**, *9*, 2704-2710.
38. King, A. R.; Lodola, A.; Carmi, C.; Fu, J.; Mor, M.; Piomelli, D. A critical cysteine residue in monoacylglycerol lipase is targeted by a new class of isothiazolinone-based enzyme inhibitors. *Br. J. Pharmacol.* **2009**, *157*, 974-983.

39. Jagerovic, N.; Fernandez-Fernandez, C.; Goya, P. CB1 cannabinoid antagonists: structure-activity relationships and potential therapeutic applications. *Curr. Top. Med. Chem.* **2008**, *8*, 205-230.
40. Domcke, S.; Sinha, R.; Levine, D. A.; Sander, C.; Schultz, N. Evaluating cell lines as tumour models by comparison of genomic profiles. *Nat. Commun.* **2013**, *4*, 2126.
41. Kinsey, S. G.; Long, J. Z.; O'Neal, S. T.; Abdullah, R. A.; Poklis, J. L.; Boger, D. L.; Cravatt, B. F.; Lichtman, A. H. Blockade of endocannabinoid-degrading enzymes attenuates neuropathic pain. *J. Pharmacol. Exp. Ther.* **2009**, *330*, 902-910.
42. Kinsey, S. G.; Long, J. Z.; Cravatt, B. F.; Lichtman, A. H. Fatty acid amide hydrolase and monoacylglycerol lipase inhibitors produce anti-allodynic effects in mice through distinct cannabinoid receptor mechanisms. *J Pain* **2010**, *11*, 1420-1428.
43. Ignatowska-Jankowska, B. M.; Ghosh, S.; Crowe, M. S.; Kinsey, S. G.; Niphakis, M. J.; Abdullah, R. A.; Tao, Q.; ST, O. N.; Walentiny, D. M.; Wiley, J. L.; Cravatt, B. F.; Lichtman, A. H. In vivo characterization of the highly selective monoacylglycerol lipase inhibitor KML29: antinociceptive activity without cannabimimetic side effects. *Br. J. Pharmacol.* **2014**, *171*, 1392-1407.
44. Wilkerson, J. L.; Niphakis, M. J.; Grim, T. W.; Mustafa, M. A.; Abdullah, R. A.; Poklis, J. L.; Dewey, W. L.; Akbarali, H.; Banks, M. L.; Wise, L. E.; Cravatt, B. F.; Lichtman, A. H. The selective monoacylglycerol lipase inhibitor MJN110 produces opioid-sparing effects in a mouse neuropathic pain model. *J. Pharmacol. Exp. Ther.* **2016**, *357*, 145-156.
45. Khasabova, I. A.; Yao, X.; Paz, J.; Lewandowski, C. T.; Lindberg, A. E.; Coicou, L.; Burlakova, N.; Simone, D. A.; Seybold, V. S. JZL184 is anti-hyperalgesic in a murine model of cisplatin-induced peripheral neuropathy. *Pharmacol. Res.* **2014**, *90*, 67-75.
46. Khasabova, I. A.; Khasabov, S.; Paz, J.; Harding-Rose, C.; Simone, D. A.; Seybold, V. S. Cannabinoid type-1 receptor reduces pain and neurotoxicity produced by chemotherapy. *J. Neurosci.* **2012**, *32*, 7091-7101.

47. Gregg, R. W.; Molepo, J. M.; Monpetit, V. J.; Mikael, N. Z.; Redmond, D.; Gadia, M.; Stewart, D. J. Cisplatin neurotoxicity: the relationship between dosage, time, and platinum concentration in neurologic tissues, and morphologic evidence of toxicity. *J. Clin. Oncol.* **1992**, *10*, 795-803.
48. Chimenti, F.; Fioravanti, R.; Bolasco, A.; Chimenti, P.; Secci, D.; Rossi, F.; Yanez, M.; Orallo, F.; Ortuso, F.; Alcaro, S. Chalcones: a valid scaffold for monoamine oxidases inhibitors. *J. Med. Chem.* **2009**, *52*, 2818-2824.
49. Starosyla, S. A.; Volynets, G. P.; Lukashov, S. S.; Gorbatiuk, O. B.; Golub, A. G.; Bdzhola, V. G.; Yarmoluk, S. M. Identification of apoptosis signal-regulating kinase 1 (ASK1) inhibitors among the derivatives of benzothiazol-2-yl-3-hydroxy-5-phenyl-1,5-dihydro-pyrrol-2-one. *Bioorg. Med. Chem.* **2015**, *23*, 2489-2497.
50. Aghazadeh Tabrizi, M.; Baraldi, P. G.; Ruggiero, E.; Saponaro, G.; Baraldi, S.; Romagnoli, R.; Martinelli, A.; Tuccinardi, T. Pyrazole phenylcyclohexylcarbamates as inhibitors of human fatty acid amide hydrolases (FAAH). *Eur. J. Med. Chem.* **2015**, *97*, 289-305.
51. Jasial, S.; Hu, Y.; Bajorath, J. How frequently are pan-assay interference compounds active? Large-scale analysis of screening data reveals diverse activity profiles, low global hit frequency, and many consistently inactive compounds. *J. Med. Chem.* **2017**, *60*, 3879-3886.
52. Baell, J. B.; Holloway, G. A. New substructure filters for removal of pan assay interference compounds (PAINS) from screening libraries and for their exclusion in bioassays. *J. Med. Chem.* **2010**, *53*, 2719-2740.
53. Dahlin, J. L.; Nissink, J. W.; Strasser, J. M.; Francis, S.; Higgins, L.; Zhou, H.; Zhang, Z.; Walters, M. A. PAINS in the assay: chemical mechanisms of assay interference and promiscuous enzymatic inhibition observed during a sulfhydryl-scavenging HTS. *J. Med. Chem.* **2015**, *58*, 2091-2113.

54. Granchi, C.; Rizzolio, F.; Bordoni, V.; Caligiuri, I.; Manera, C.; Macchia, M.; Minutolo, F.; Martinelli, A.; Giordano, A.; Tuccinardi, T. 4-Aryliden-2-methyloxazol-5(4H)-one as a new scaffold for selective reversible MAGL inhibitors. *J. Enzym. Inhib. Med. Ch.* **2016**, *31*, 137-146.
55. Dahlin, J. L.; Walters, M. A. How to triage PAINS-full research. *Assay Drug Dev. Technol.* **2016**, *14*, 168-174.
56. Del Carlo, S.; Manera, C.; Chicca, A.; Arena, C.; Bertini, S.; Burgalassi, S.; Tampucci, S.; Gertsch, J.; Macchia, M.; Saccomanni, G. Development of an HPLC/UV assay for the evaluation of inhibitors of human recombinant monoacylglycerol lipase. *J. Pharm. Biomed. Anal.* **2015**, *108*, 113-121.
57. Case, D. A.; Berryman, J. T.; Betz, R. M.; Cerutti, D. S.; III, T. E. C.; Darden, T. A.; Duke, R. E.; Giese, T. J.; Gohlke, H.; Goetz, A. W.; Homeyer, N.; Izadi, S.; Janowski, P.; Kaus, J.; Kovalenko, A.; Lee, T. S.; LeGrand, S.; Li, P.; Luchko, T.; Luo, R.; Madej, B.; Merz, K. M.; Monard, G.; Needham, P.; Nguyen, H.; Nguyen, H. T.; Omelyan, I.; Onufriev, A.; Roe, D. R.; Roitberg, A.; Salomon-Ferrer, R.; Simmerling, C. L.; Smith, W.; Swails, J.; Walker, R. C.; Wang, J.; Wolf, R. M.; Wu, X.; York, D. M.; Kollman, P. A. *AMBER*, version 14; University of California: San Francisco, CA, 2015.
58. *Maestro*, version 9.0; Schrödinger Inc: Portland, OR, 2009.
59. *Macromodel*, version 9.7; Schrödinger Inc: Portland, OR, 2009.
60. Morris, G. M.; Goodsell, D. S.; Halliday, R. S.; Huey, R.; Hart, W. E.; Belew, R. K.; Olson, A. J. Automated docking using a Lamarckian genetic algorithm and an empirical binding free energy function. *J. Comput. Chem.* **1998**, *19*, 1639-1662.
61. Morris, G. M.; Huey, R.; Lindstrom, W.; Sanner, M. F.; Belew, R. K.; Goodsell, D. S.; Olson, A. J. AutoDock4 and AutoDockTools4: Automated docking with selective receptor flexibility. *J. Comput. Chem.* **2009**, *30*, 2785-2791.

62. Chicca, A.; Caprioglio, D.; Minassi, A.; Petrucci, V.; Appendino, G.; Tagliatela-Scafati, O.; Gertsch, J. Functionalization of beta-caryophyllene generates novel polypharmacology in the endocannabinoid system. *ACS Chem. Biol.* **2014**, *9*, 1499-1507.
63. Cavaletti, G.; Tredici, G.; Petruccioli, M. G.; Donde, E.; Tredici, P.; Marmiroli, P.; Minoia, C.; Ronchi, A.; Bayssas, M.; Etienne, G. G. Effects of different schedules of oxaliplatin treatment on the peripheral nervous system of the rat. *Eur. J. Cancer* **2001**, *37*, 2457-2463.
64. Di Cesare Mannelli, L.; Lucarini, E.; Micheli, L.; Mosca, I.; Ambrosino, P.; Soldovieri, M. V.; Martelli, A.; Testai, L.; Tagliatela, M.; Calderone, V.; Ghelardini, C. Effects of natural and synthetic isothiocyanate-based H₂S-releasers against chemotherapy-induced neuropathic pain: Role of Kv7 potassium channels. *Neuropharmacology* **2017**, *121*, 49-59.
65. Di Cesare Mannelli, L.; Pacini, A.; Bonaccini, L.; Zanardelli, M.; Mello, T.; Ghelardini, C. Morphologic features and glial activation in rat oxaliplatin-dependent neuropathic pain. *J. Pain* **2013**, *14*, 1585-1600.

TABLE OF CONTENTS GRAPHIC

